buildings

MDPI

Article

Damage Identification in Reinforced Concrete Beams Using Wavelet Transform of Modal Excitation Responses

Atefeh Soleymani [1], Hashem Jahangir [2,*], Maria Rashidi [3,*], Farid Fazel Mojtahedi [4], Michael Bahrami [5] and Ahad Javanmardi [3,6]

[1] Department of Civil Engineering, Shahid Bahonar University of Kerman, Kerman 7616913439, Iran; atefeh_soleymani@eng.uk.ac.ir
[2] Department of Civil Engineering, University of Birjand, Birjand 9717434765, Iran
[3] Centre for Infrastructure Engineering, Western Sydney University, Sydney, NSW 2000, Australia; ahad@fzu.edu.cn
[4] Department of Infrastructure Engineering, University of Melbourne, Parkville, VIC 3010, Australia; farid.fazelmojtahedi@unimelb.edu.au
[5] Department of Civil Engineering, Sharif University of Technology, Tehran 1458889694, Iran; meikaeil.bahrami@sharif.edu
[6] College of Civil Engineering, Key Lab of Fujian Province, Fuzhou University, University Town, 2 Xueyuan Road, Fuzhou 350108, China
* Correspondence: h.jahangir@birjand.ac.ir (H.J.); m.rashidi@westernsydney.edu.au (M.R.)

Abstract: This study focuses on identifying damage in reinforced concrete (RC) beams using time-domain modal testing and wavelet analysis. A numerical model of an RC beam was used to generate various damage scenarios with different severities and locations. Acceleration time histories were recorded for both damaged and undamaged structures. Two damage indices, *DI_MW* and *DI_SW*, derived from the wavelet analysis, were employed to determine the location and severity of the damage. The results showed that different wavelet families and specific mother wavelets had varying effectiveness in detecting damage. The Daubechies wavelet family (db2, db6, and db9) detected damage at the center and sides of the RC beams due to good time and frequency localization. The Biorthogonal wavelet family (bior2.8 and bior3.1) provided improved time–frequency resolution. The Symlets wavelet family (sym2 and sym7) offered a balanced trade-off between time and frequency localization. The Shannon wavelet family (shan1-0.5 and shan1-0.1) exhibited good time localization, while the Frequency B-Spline wavelet family (fbsp2-1-0.1) excelled in frequency localization. Certain combinations of mother wavelets, such as shan1-0.5 with the *DI_SW* index, were highly effective in detecting damage. The *DI_SW* index outperformed *DI_MW* across different numerical models. Selecting appropriate wavelet analysis techniques, particularly utilizing shan1-0.5 in the *DI_SW*, proved effective for detecting damage in RC beams.

Keywords: damage localization; damage severities; modal excitation responses; time domain; reinforced concrete beams

Citation: Soleymani, A.; Jahangir, H.; Rashidi, M.; Mojtahedi, F.F.; Bahrami, M.; Javanmardi, A. Damage Identification in Reinforced Concrete Beams Using Wavelet Transform of Modal Excitation Responses. *Buildings* **2023**, *13*, 1955. https://doi.org/10.3390/buildings13081955

Academic Editor: Piero Colajanni

Received: 16 July 2023
Revised: 28 July 2023
Accepted: 29 July 2023
Published: 31 July 2023

1. Introduction

Contemporary societies face risks posed by aging civil constructions, natural disasters, environmental factors, and extreme loads. Structural health monitoring (SHM) has become an essential aspect in ensuring structural integrity, safety, and cost-effective maintenance [1,2]. SHM systems have been widely used to detect and monitor "damage-sensitive characteristics" for timely assessments and continuous evaluation. The goal is to achieve comprehensive system state awareness from construction to retirement [3,4].

Structural damage can decrease the load-bearing capacity of buildings, disrupt normal operations, and eventually lead to structural collapse. Therefore, in recent decades, the field of structural safety has placed significant emphasis on identifying potential structural failures. The development of effective methods for evaluating damage to structural members is crucial for preventing catastrophic engineering incidents. To this end, several techniques have been developed recently to detect structural flaws by analyzing modifications in structural response parameters, for instance, changes in static shear energy [5]. Typically, changes in damage-sensitive characteristics are measured using "damage indicators". Examples of such indicators include the T2 gauge [6] and the modal assurance criterion (MAC) [7], which are mathematical functions that are based on these properties but do not have a clear physical interpretation. Varying with the technique implemented for damage identification and the available data, damage can be recognized at varying degrees of sophistication. This includes the detection, quantification, and localization of damage [8]. Damage localization and quantification provide supplementary information regarding the position and severity of the damage, respectively, while damage detection provides a binary outcome by indicating whether the damage is present or not. Novel methods, such as Multiple Linear Regression, Linear PCA, Local PCA, and others, are commonly used for detecting damage in civil structures, like bridges. These methods often provide a binary outcome [6], historical landmarks, and particular structural components [7].

By modifying the Power Spectral Density (PSD) configuration, the features stated by Le-Ngoc et al. [9] were modified by Le-Ngoc and his team to indicate structural degradation. The researchers noted alterations in the power spectrum resulting from the vibrations of beams that had experienced structural damage as a result of moving loads. These findings have led to the proposal of monitoring measures for the detection of structural deterioration. In addition, Le-Ngoc and his team reasoned that employing PSD shape changes will improve the capability to discover the damage in beam-like structures, a long, slender construction used for support and load distribution [9]. In the study of Peng and Yang [5], a static shear energy approach was introduced for inspecting destruction in beam-like structures and identifying the specific locations of the damage. According to the energy release theory, when structural damage occurs, the strain energy of a damaged section quickly changes. Hanumanthappa [10] asserted that the utilization of natural frequencies and mode shapes is prevalent in identifying structural degradation due to their precise measurement capabilities and sensitivity to regional damage. The accuracy of damage localization might be jeopardized by measurement mistakes, which can make it challenging to determine mode shapes. Hanumanthappa [10] put up the Generalized Flexibility Quotient Difference method for cantilever beams as a fresh solution to this problem. This approach can accurately detect damage in both individual and multiple beam components, distinguishing between two levels of damage severity. It achieves this detection with only two stages. The suggested damage index is calculated by using the stiffness matrix of the undamaged component rather than the stiffness matrix of the damaged part. The effectiveness of the proposed damage detection technique was tested using six different damage scenarios. Nguyen [11] proposed a new indicator for assessing structural changes, which is based on changes in the center position of the probability spectrum of a vibration signal, referred to as the change in the probability spectrum center (C-PSD). The author argued that this approach can improve the sensitivity of the model to structural changes. Furthermore, a distinctive aspect of the methodology is its reliance on the natural frequency center as the sole criterion for evaluating the damaged structure, deviating from the conventional approach that incorporates multiple natural frequencies. Therefore, this more sensitive indicator based on C-PSD is expected to be more effective in analyzing and detecting structural damages than previous indicators presented just based on basic statistical parameters, including the average and standard deviation. Huang et al. [12] used a mechanics-driven statistical moment feature of wavelet transform-processed dynamic responses to suggest a technique for detecting various kinds of damage in beam-type structures. CWT, which stands for continuous wavelet transform, is used to represent the feature of analyzing the second-order strain statistical moment (SSSM). Data fusion technology and the Three-Sigma Rule in statistics are utilized to create a damage index by collecting and enlarging the damage singularities brought on by damage using a CWT at an every-order SSSM curve. Damage is present when the damage index abruptly changes. The study demonstrated that the suggested characteristic, even under roughly uniform spectral excitations, is resistant to noise and can correctly detect a large number of fractures without the requirement for baseline data on the undamaged counterpart. Pooya and Massumi [13] developed a damage detection approach specifically designed for beam-like structures that can locate the damage, utilizing just the dynamic data of the damaged structure. As a marker for the damage location in the beam's constituent elements, the discrete segments used in a finite element analysis, the technique determines the actual difference between a coefficient of the modal strain energy of one element and then a coefficient of the modal kinetic energy of either that component or another component of that beam. Neither mechanical nor geometric information from the cracked beam or the base model is used in the proposed technique; rather, just modal movements and the length of the damaged beam sections are needed. A finite element model of damaged beams with varied geometries and boundary conditions was used to show the method's capacity to identify the damage, and the findings were confirmed using dynamic testing.

Vibration-based structural health monitoring (VSHM) is a method used to evaluate the occurrence, position, and magnitude of harm in composite structures, such as buildings. This is achieved by examining the vibration information obtained from the structure [14–16]. The VSHM technique estimates the vibrational changes caused by damage by utilizing diverse vibration attributes, such as mode shapes, the modal damping ratio, and modal frequencies. Different VSHM methods are developed based on the diversity and combination of vibration parameters, such as modal flexibility, modal stiffness, and strain energy. However, all VSHM approaches rely on the principle that any alteration in a structure's mechanical or geometrical features will affect its dynamic characteristics [17]. VSHM techniques are non-destructive and have the ability to identify the precise location and intensity of damage without requiring any prior knowledge. Several VSHM techniques have been proposed, including those focused on a structure's modal characteristics, for instance, mode shapes [18] and natural frequencies [19], as well as those that use frequency response functions (FRFs) and vibration response in the time or frequency domain [20]. The techniques used in VSHM can be broadly classified into two categories: model-based and non-model-based methods [21]. Model-based approaches involve comparing observed and simulated vibration responses to identify damage and minimize the difference between the two. In contrast, non-model-based approaches do not depend on models or assumptions about a structure's vibratory response. Instead, they solely rely on the measurement of vibration response using techniques, like pure data analysis, time series analysis, and/or natural frequencies [22].

The experimental investigation of a vibration-based damage diagnosis system for a 2.5-dimensional composite structure was conducted by Ooijevaar et al. [23]. The researchers employed the modal strain energy damage index (MSEDI) technique, which integrated both bending and torsion modes in its methodology. Based on experimental data obtained from a measurement device used to assess the dynamic behavior, it was observed that bending vibrations can lead to delamination in a composite T-beam structure, which can be detected using the MSEDI method. Changes in the natural frequencies of bending modes serve as a reliable indicator for the presence of delamination within a structure. The fourth- and higher-order bending mode shapes, along with the damage index algorithm, can also forecast the location and magnitude of the damages. The research conducted by Loendersloot et al. [24] investigated an FE-based numerical model for a vibration-based damage detection technique for a thin-walled slender composite structure. An analysis was performed on the linear dynamic response of a 16-layer unidirectional carbon fiber-reinforced PEKK T-beam that was both intact and partially delaminated. Using the bending and torsion modes of the structure, the MSEDI algorithm's ability to locate and detect delamination was evaluated. Jyrki et al. [25] investigated the VSHM of a (FE) model of a simply supported beam that contained pre-existing cracks. They employed a sensor array to monitor the structure, which measured transverse acceleration in response to random stimulation. The primary objective was to ascertain the minimum crack length that could be detected and identified. Additionally, the effect of sensor placement was investigated. Following the Generalized Likelihood Ratio Test (GLRT), principal component analysis (PCA) was utilized for damage identification in the time domain. It was discovered that a crack could be seen at the bottom of the beam's center when its length approached 10% of the beam's height. Using the monitoring data, the precise location of the crack was determined. In an experimental study, Ho and Thanh-Cao [26] introduced intelligent techniques utilizing vibration and impedance for structural health monitoring (SHM) of prestressed concrete (PSC) beams. The following methods were employed to accomplish the goal or aim. Primarily, the hardware and embedded software of intelligent sensors were specifically engineered to facilitate the surveillance of vibration patterns and impedance characteristics. The design proposed a novel sensor network, how to place the sensors on the surface of the structures, for measuring the dynamic strain measured by piezoelectric transducers (PZT). The experimental recordings of vibration and impedance responses from a PSC beam were analyzed to validate the viability of smart sensors for SHM. At least two behavior patterns of the PSC beam were investigated: (1) the relationship between the vibration of the girder and the vibration of the cable and (2) the impact of wind velocities on the beam's vibration and impedance behavior.

The majority of traditional damage detection techniques in structural health monitoring (SHM) rely on analyzing the frequency characteristics and structural stiffness. The fast Fourier transform (FFT) is commonly employed for this type of analysis. However, in recent years, the wavelet transform has gained prominence as being highly promising for SHM. This technique, which is an improvement over the traditional Fourier transform, has demonstrated its efficacy in SHM applications [27]. The capability of wavelet transform to analyze vibration signals was first identified by Newland [28]. Several researchers, including Wang and McFadden [29] and Surace and Ruotolo [30], applied the wavelet transform in the time domain for damage identification through vibration signal analysis. Salehian et al. [31] recently used the wavelet method to detect abruptly induced structural damage in a plate. The response data were collected at multiple sensor points after simulating the damage as an impulse signal, and the wavelet transform was used to determine the travel times from the impact location to the sensor locations to locate the damage. Yan and Yam [32] investigated delamination damage in a composite laminated plate by utilizing embedded piezoelectric patches. The wavelet analysis was used to define the energy fluctuation in the dynamic response of the structure, and damage was detected based on this fluctuation. Y. Huang et al. [27] conducted a study where they developed a distributed method for two-dimensional (2D) continuous wavelet transform (CWT). This method effectively monitors structural deterioration by utilizing information from discrete sets of nodes. It provides continuous spatial changes in the parameters associated with the structural response. This method can be utilized for SHM by coupling it using a network of embedded sensors capable of supplying signals of nodal responses.

The authors emphasized the algorithm's merits, which encompass its reliance on local data, its ability to provide spatially continuous information, and its minimal requirements in terms of connectivity and computational resources. The damage locations and intensity can be accurately identified and qualitatively evaluated. To demonstrate the potential use of a three-dimensional (3D) CWT for structural health monitoring (SHM), Shi and Yu [33] examined a 3D data scenario involving a 2D spatial signal with time history. Additionally, Shi and Yu [33] explored the use of the combination of artificial neural networks (ANNs) and wavelet analysis to create a smart and adaptable system for detecting structural damage. Fallahian et al. [34] proposed a system for detecting structural damage that employed a combination of the discrete wavelet transform (DWT) and a series of pattern recognition models. The data from vibrations were decomposed using the discrete wavelet transform, and principal component analysis was applied to reduce the decomposed data. The compressed and decomposed vibration data along with damage data were subsequently employed to train separate damage models of the building. They utilized pattern recognition models based on deep neural networks and coupled sparse coding. The individual damage models were combined into a single model using a majority voting approach, in order to predict the position and severity of structural damage. The algorithm was found to accurately detect initial damages in many locations, even in complex structures and beam-column connections, in situations where uncertainty, such as noise and temperature fluctuations, was present. Kaur et al. [35] proposed a comprehensive approach for identifying, evaluating, and localizing structural damage using an unsupervised adversarial autoencoder and wavelet transform. The authors trained the adversarial autoencoder model using only vehicle acceleration data obtained from a healthy bridge state. They employed an estimated reconstruction error-based damage detection index and utilized signal averaging and spectrum filtering pre-processing techniques to improve the model's performance. Additionally, wavelet transform and signal pre-processing methods were used to predict the locations of detected defects. The proposed method was demonstrated to be effective in identifying damages of varying degrees and accurately localizing them. Pradeep et al. [36] proposed a method based on wavelet transform to detect structural damage in plates. The authors utilized a continuous wavelet transform to detect signal discontinuities in mode shape displacement. Their approach enabled the identification of damage sources on a plate structure at any location in the building. Moreover, the method yielded a dependable output for damage identification using a single-mode shape, compared to frequency analysis. Ruan et al. [37] utilized artificial neural network (ANN) models to find the relationship between the responses of the structures and the amount of stiffness reduction caused by damages. In their study, random acceleration and displacement were considered as the input parameters and the severities of the damages were the output parameters in the proposed ANN models. Their proposed ANN models successfully detected the damage severities in a five-story building structure.

2. Research Significance

Most of the research on damage detection has utilized a frequency-domain analysis of modal data, as revealed by the literature review conducted in the fields of damage detection and structural health monitoring. Although the modal data in the frequency domain are more compatible with the mechanical properties of structures and are easier to analyze, due to their accurate representation of mode shapes, they are highly preferred for damage detection and structural health monitoring applications, facilitating frequency-dependent analysis, exploiting the linearity assumption, and exhibiting high sensitivity to structural changes. Meanwhile, the transmission from the time domain to the frequency domain can be performed accurately, as analyzing the intact modal data in the time domain provides more precise outcomes for assessing the damage status of structures. This approach eliminates potential uncertainties and assumptions associated with frequency-domain transformations, allowing for a direct assessment of the structural response. This paper proposes an automated approach for damage detection in a reinforced concrete (RC) beam using a combination of time-domain modal testing and wavelet transform analysis. The method aims to overcome the limitations of traditional approaches by providing an accurate and efficient means of damage localization and severities in RC beams. By using a numerical model of an RC beam, different damage scenarios with varying degrees of severity were created to simulate the effects of structural deterioration. During the modal test, acceleration time histories were recorded. The inputs for the wavelet analyses included data obtained from time-domain modal testing for both the structures with and without damage. The proposed approach uses 14 wavelet families with a total of 84 mother wavelets. It calculates two damage indices, *DI_MW* and *DI_SW*, based on the maximum values of detail coefficients and the area under the detail coefficients diagram obtained from the wavelet transform. These indices help determine the location and severity of the damage scenarios. Eventually, the best mother wavelet was selected based on the capability to identify the location and quantify the severity of impact for all damage scenarios at different locations.

3. Selected Wavelet Families

Wavelets, which are mathematical functions, are employed in signal processing to analyze signals by using variable-sized windows through a time transformation process. This method prioritizes brief time periods for high-frequency elements and extended time periods for low-frequency elements, allowing for the accentuation of local changes in the signal [38]. Instead of frequency, in wavelet transform, a reciprocal scale factor (s) is employed to modulate the wavelets utilized in the decomposition of the input function ensemble into a succession of progressively scaled and translated wavelets, with each wavelet referred to as a mother wavelet, denoted by $\psi(x)$ [39]. The wavelet transform employs a mathematical function $\psi(t, a, b)$ to rescale and shift the mother wavelet:

$$\psi(t, s, b) = \frac{1}{\sqrt{s}} \psi\left(\frac{t-b}{s}\right) \tag{1}$$

In Equation (1), the parameters s and b denote the scaling and translational transformations, respectively, and the transformation can be parameterized by scaling and translating the wavelet coefficients. An example of wavelet scaling is the modification of the wavelet's length through compression or stretching; when a wavelet is translated, it will initiate with a time delay [39]. The continuous wavelet transform (CWT), also referred to as the wavelet transform, consists of multiplying the whole signal by the wavelet function and then applying scaling and translation operations to $\psi(t, a, b)$:

$$CWT(s, b) = \int_{-\infty}^{\infty} f(t) \cdot \psi(t, s, b) dt \tag{2}$$

The wavelet coefficients establish a connection between the wavelet function and the original signal, indicating the extent to which they are alike or resemble each other. As coefficients increase, the shape of the wavelets becomes more similar to that of the input signal. The wavelet transformation involves decomposing the signal into different scales and positions, resulting in a multi-resolution analysis. At each scale, the wavelet coefficients capture the details and characteristics of the signal within that particular scale. As a result, the calculation of coefficients generates a substantial amount of data, regardless of the scale; the reduction in scale can be achieved through the utilization of dyadic scales and positions that effectively harness the exponential power of two, commonly known as dyadic scales and positions. The discrete wavelet transform (DWT) is a method for examining discrete data. Mallat's research [38] established that filter analysis, commonly referred to as fast-transforming wavelets, has emerged as a prominent technique. By utilizing this technique, which utilizes the initial signal as an input, it becomes possible to produce the wavelet coefficient as the resulting output. As a result, this transformation produces the wavelet function:

$$\psi_{j,k}(t) = \frac{1}{\sqrt{2^j}} \psi(\frac{t - 2^j k}{2^j}) = 2^{-j/2} \psi(2^{-j} t - k) \tag{3}$$

Equation (3) determines the decomposition level j, using both time t and scale 2^j as input parameters. The discrete wavelet coefficients are computed based on Equation (4), which includes the operation of multiplying the $f(t)$ signal by the translated and scaled wavelet $\psi_{j,k}(t)$:

$$DWT(j, k) = \int_{-\infty}^{\infty} f(t) \cdot \psi_{j,k}(t) dt \tag{4}$$

The discrete wavelet transformation involves applying a low-pass and high-pass filter to the original signal. The filters are linear operators. Low-pass filters smooth out signal singularities, while high-pass filters highlight singularities and reduce smooth regions [40]. Considering approximation coefficients as low-frequency signals with a higher scale and regarding high-scale components as details can be a beneficial approach. By utilizing a wavelet to filter the primary signal, it is feasible to isolate these components, and the process of decomposing the approximation coefficients can proceed in a sequence. As a result of this process, a considerable number of components are obtained, which are isolated from the original signal. Important information can be obtained by decomposing the wavelet tree which is a binary tree data structure that efficiently represents the frequency components of a sequence or array, enabling wavelet-based operations and computations. At each level of the tree, coefficients for signal approximation and details can be discovered. In the DWT, a non-continuous wavelet pattern is created by a linear combination of the wavelet function $\psi(t)$ with the scaling function $\phi(x)$. This is in contrast to the CWT, where only the wavelet function is utilized. The scaling function is associated with low-pass filters, while high-pass filters are associated with the wavelet function. Using the scaling function is analogous to utilizing the wavelet function. Wavelet coefficients furnish a detailed depiction of the primary signal, whereas scaling coefficients produce an approximate depiction. There are no scaling functions for the wavelets other than the orthogonal ones [41].

As reported in Table 1, wavelets can be categorized into several families, in which each family contains mother wavelets based on their features relevant to signal processing, for instance, the degree of smoothness, and symmetry [38]. The wavelet families including Gaussian, Mexican, Shannon, and Morlet do not possess distinct wavelet properties in their ψ function. They also lack a scaling function $\varnothing$, which prevents the conversion of discrete wavelets and their reconstruction. On the other hand, Haar, Daubechies, and Coiflet wavelets, among other families, do not have a prominent ψ function. However, they include a scaling function ϕ, allowing for the use of discrete wavelets. These wavelets are slightly asymmetrical and exhibit moderate regularity. On the contrary, the Biorthogonal wavelets and Reverse Biorthogonal wavelets are types of wavelets that are capable of being reconstructed with symmetrical and precise properties. Furthermore, Biorthogonal wavelets and Reverse Biorthogonal wavelets have two separate wavelet and scaling functions. Typically, before determining which wavelet to utilize, a process of trial and error is required.

Table 1. The wavelet families and their related mother wavelets.

Wavelet Families	Nomenclature	Mother Wavelets
Daubechies	db	db1 = haar, db2, db3, db4, db5, db6, db7, db8, db9, db10
Symlets	sym	sym2, sym3, sym4, sym5, sym6, sym7, sym8
Coiflets	coif	coif1, coif2, coif3, coif4, coif5
BiorSplines	bior	bior1.1, bior1.3, bior1.5, bior2.2, bior2.4, bior2.6, bior2.8, bior3.1, bior3.3, bior3.5, bior3.7, bior3.9, bior4.4, bior5.5, bior6.8
ReverseBior	rbio	rbio1.1, rbio1.3, rbio1.5, rbio2.2, rbio2.4, rbio2.6, rbio2.8, rbio3.1, rbio3.3, rbio3.5, rbio3.7, rbio3.9, rbio4.4, rbio5.5, rbio6.8
Meyer	meyr	meyr
Dmeyer	dmey	dmey
Gaussian	gaus	gaus1, gaus2, gaus3, gaus4, gaus5, gaus6, gaus7, gaus8
Mexican_hat	mexh	mexh
Morlet	morl	morl
Complex Gaussian	cgau	cgau1, cgau2, cgau3, cgau4, cgau5
Shannon	shan	shan1-1.5, shan1-1, shan1-0.5, shan1-0.1, shan2-3
Frequency B-Spline	fbsp	fbsp1-1-1.5, fbsp1-1-1, fbsp1-1-0.5, fbsp2-1-1, fbsp2-1-0.5, fbsp2-1-0.1
Complex Morlet	cmor	cmor1-1.5, cmor1-1, cmor1-0.5, cmor1-0.1

In this paper, as presented in Table 1, 14 wavelet families including 84 mother wavelets were selected to identify damage scenarios in RC beams by analyzing the modal excitation forces obtained from the numerical models conducted based on selected experiments from a previous study conducted by Baghiee et al. [42]. Table A1 in Appendix A outlines the characteristics of all the wavelet families and mother wavelets considered in this paper.

4. Assessing the Location and Severities of Damage Scenarios

4.1. Experimental-Based Numerical Models

In this paper, one of the RC beams tested previously by Baghiee et al. [42] was selected to build the numerical model. In their study, the experimental procedure involved subjecting the specimens to incremental static bending tests to induce gradual damage, and after each set of static loading, modal analysis was utilized to obtain the dynamic characteristics with the specimens suspended to mitigate the impact of support and floor vibrations. In the conducted experiments, the independent variables were determined along the principal axis of the specimen's top surface. These variables were spaced at fixed intervals of 100 mm, resulting in a total of 23 variables. They were referred to as degrees of freedom (DOFs) [42]. In the process of conducting modal tests, the frequency response functions (FRFs) were acquired through the utilization of time-domain measurements of the impulse force and the responses of the specimens, which were then projected onto the frequency domain. The impact forces were measured by designated sensors positioned atop the impact hammer. The recorded output measurements were obtained via piezoelectric sensors that were attached to the structural component to capture the vibratory reactions. Although the impact hammer was exerted on all degrees of freedom, the affixed sensor could be immobilized at a particular location on the structural member. The geometric and mechanical properties of the aforementioned RC beam are detailed in Figure 1. More details regarding the experimental tests can be found in [43].

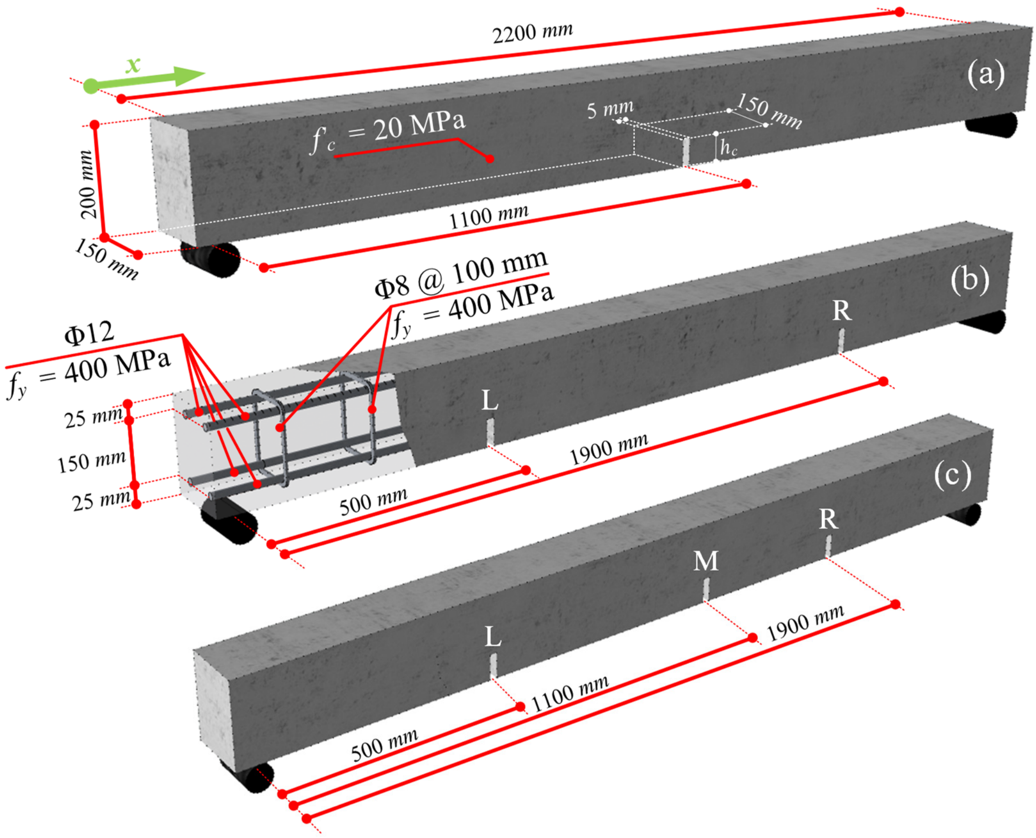

Figure 1. The geometrical and mechanical properties of the RC beam numerical model, including different damage scenarios perpendicular to the *x*-axis: (**a**) single, (**b**) double, and (**c**) triple.

Using ABAQUS software [44], a computational simulation of the experimental RC beam specimen was developed utilizing a 3D approach. The geometrical and mechanical properties of the numerical model are illustrated in Figure 1, including the height of cracks (h_c), compressive strength of concrete (f'_c), and yield stress of steel bars (f_y). In this model, the modulus of elasticity, density, and Poisson ratio for the concrete and steel materials were considered to be 17 and 200 GPa, 2400 and 7850 kg/m^3, and 0.17 and 0.3, respectively. The boundary conditions in the computational model were hypothesized to be congruent with the suspended condition test, and the frequencies of the numerical investigation and experimental specimen exhibited a high degree of similarity, which are, respectively, 114.28 and 114.28 Hz for the first mode, 298.42 and 304.89 Hz for the second mode, and 560.24 and 563.19 Hz for the third mode. More finite element method (FEM) details of the numerical model as well as its verification based on the experimental RC beam can be found in [43].

As presented in Table 2, Three damage scenarios indicated as single (S), double (D), and triple (T) were created in the model by applying artificial cracks (slots) with a constant width (5 mm) and variant height values (h_c) located at the left (L), middle (M), and right (R) of the RC beam. Three distinct height values, namely, 3 mm, 6 mm, and 10 mm, were examined and designated as C_r (crack ratio). These values were determined based on their respective ratios to the cross-sectional height of the beam (200 mm), resulting in percentages of 15%, 30%, and 50%. As a result, three individual damage scenarios were identified, positioned on the left, middle, and right sides of the RC beam, respectively, named S_L, S_M, and S_R, and three double-damage scenarios located on the left and right, left and middle, and middle and right sides of the RC beam, respectively, named D_LR, D_LM, and D_MR, and a triple-damage scenario, named T_LMR, were studied.

Table 2. The features of damage scenarios.

Damage Scenario	Crack (Slot) Location	x (mm)	Abbreviations
Single	Left	500	S_L
	Middle	1100	S_M
	Right	1900	S_R
Double	Left and Right	500 and 1900	D_LR
	Left and Middle	500 and 1100	D_LM
	Middle and Right	1100 and 1900	D_MR
Triple	Left, Middle, and Right	500, 1100 and 1900	T_LMR

As illustrated in Figure 2, the degrees of freedom (DOFs) were arranged uniformly at intervals of 100 mm, in accordance with the modal tests performed during the experiment. Consequently, the numerical model of the selected RC beam comprised a total of 23 DOFs.

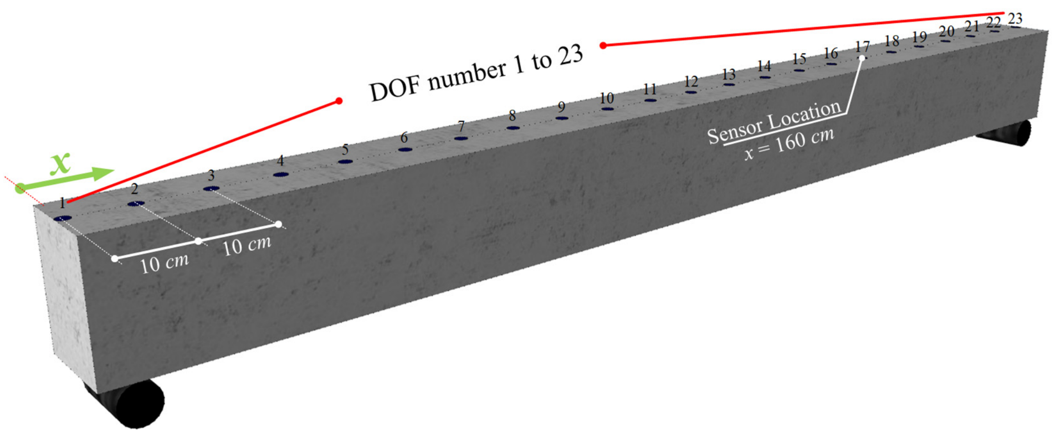

Figure 2. Considered degrees of freedom (DOFs) on the numerical RC beam model.

This paper aimed to evaluate the attributes of the numerical models for modal testing on the RC beam through impact hammer simulations. In this study, percussive impacts were applied individually to each degree of freedom (DOF). Moreover, in addition to calculating and simultaneously measuring the magnitude of forces generated on each DOF by the hammer, a piezoelectric sensor was utilized to record the accelerations resulting from the applied impacts, specifically at DOF number 17 (x = 160 cm). As illustrated in

Figure 3, the force-time diagram applied by the impulsive hammer in the Pappalardo and Guida investigation [45] was utilized for this objective. The force of the impact hammer was applied on each DOF of the RC beam and, subsequently, the resulting accelerations for each DOF were ascertained using the unique sensor.

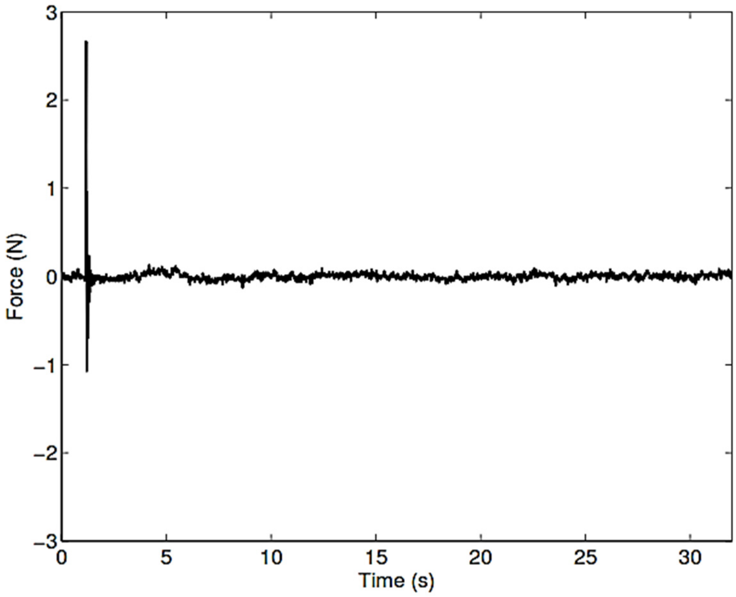

Figure 3. Time history of the impact force reported in the research of Pappalardo and Guida [45].

4.2. Damage Localization

This study proposes two novel damage indices to identify the damage location. The proposed indices rely on the analysis of acceleration time histories of the RC beams in both damaged and undamaged states. To determine the optimal wavelets for the proposed indices, a trial-and-error approach was employed, wherein 14 wavelet families including 84 mother wavelets, previously reported in Table 1, were analyzed and compared. The proposed damage indices, named *DI_MW* and *DI_SW*, were computed for each DOF (N_i) for both the damaged and undamaged conditions. This was accomplished by utilizing each of the mother wavelets to process the corresponding time histories of acceleration. The *DI_MW* and *DI_SW* were computed by taking into account the discrepancy between the peak values in the damaged (MW_D) and undamaged (MW_U) status and the integral of the corresponding detail coefficients plot for the damaged (SW_D) and undamaged (SW_U) status, as represented by Equations (5) and (6):

$$(DI\_MW)_{N_i} = \frac{(MW_D - MW_U)_{N_i}}{\max\left((MW_U)_{N_i}\right)} \tag{5}$$

$$(DI\_SW)_{N_i} = \frac{(SW_D - SW_U)_{N_i}}{\max\left((SW_U)_{N_i}\right)} \tag{6}$$

The results obtained from utilizing the suggested damage indices DI_MW and *DI_SW* across all numerical models are reported in Appendix A. The outcome values of the suggested damage indices for single-, double-, and triple-damage scenarios are documented in Table A2, Table A3 and Table A4, respectively.

The authors of the current study conducted an investigation designed to assess the efficacy of distinct wavelet families and their related mother wavelets in identifying damage scenarios by utilizing the suggested damage detection indices, *DI_MW* and *DI_SW*. The results indicate that certain mother wavelets belonging to various families exhibited superior performance in identifying damages of the modeled RC beams in the current study, as summarized in Table 3. Specifically, the db10 and fbsp1-1-0.5 mother wavelets, respectively, from the Daubechies and Frequency B-Spline wavelet families, demonstrated robustness in detecting damages when using *DI_MW*. This study's scientific rigor, reliance on established methodologies, and consideration of various wavelet families and damage scenarios enhance the generalizability of its findings. By employing finite element simulations, analyzing acceleration responses, and evaluating different mother wavelets, this study provides valuable insights applicable to a wide range of structures. Concerning *DI_SW*, some mother wavelets from the Daubechies wavelet family including db2, db6, and db9, as well as some mother wavelets from the Symlets wavelet family including sym2 and sym7, and some mother wavelets form the Biorthogonal wavelet family named bior2.8 and bior3.1 were observed. The db10 and fbsp1-1-0.5 mother wavelets from the Daubechies and Frequency B-Spline wavelet families, respectively, exhibited higher effectiveness in detecting a greater number of damage scenarios compared to other types of mother wavelets. Furthermore, the results highlight the effectiveness of the shan1-0.5, shan1-0.1, and fbsp2-1-0.1 mother wavelets from the Shannon and Frequency B-Spline wavelet families for both damage indices, *DI_MW* and *DI_SW*, as their values exceeded the corresponding values among other studied mother wavelets in the current study. This evidence emphasizes the significance of meticulously choosing a suitable wavelet to guarantee the precise identification of impairments using suggested damage indices.

Table 3. Selected best mother wavelets for damage detection based on number of detected cracks.

Damage Index	Proper Mother Wavelets
DI_MW	db10, fbsp1-1-0.5
DI_SW	db2, db6, db9, sym2, sym7, bior2.8, bior3.1
DI_MW and *DI_SW*	shan1-0.5, shan1-0.1, fbsp2-1-0.1

Numerous research studies have suggested that employing a threshold, determined through the statistical analysis of index values [46–48], can be beneficial in effectively indicating the location of identified damages when utilizing damage indices [48–50]. To this end, this paper adopts a damage threshold for improved damage location presentation. By setting a damage threshold, it is possible to differentiate between acceptable and unacceptable levels of damage and improve the accuracy of damage identification. The proposed threshold is a numerical value that serves as a cutoff point, beyond which the magnitude of the damage indices is deemed significant. The utilized damage threshold, denoted by Trα, is presented below [51]:

$$Tr_{\alpha} = \mu + Z_{\alpha}\left(\frac{\sigma}{\sqrt{n}}\right) \tag{7}$$

Equation (7) defines the mean (μ) and standard deviation (σ) of the damage index value. It also states that the standard normal distribution, represented by Z_{α}, has a mean of zero and a standard deviation of one. Furthermore, the cumulative probability of Z_{α} is equal to 100 times $(1 - \alpha)$ percent. To enhance the precision of identifying the location of damage and eliminate anomalies in the damage indices, this investigation calculates the threshold parameter (Tr_{α}) with a 95% confidence level (α = 0.05). The Trα parameter acts as a threshold for determining the severity limit of damage scenarios, and any DOF in which the value of the damage index surpasses the threshold is regarded as being damaged. Figure 4 depicts an example of the application of the threshold value on the damage index. The incorporation of a threshold value is an effective strategy to mitigate the impact of noise and other external factors on the damage identification process, enhancing the reliability of the results.

In this paper, the suggested damage threshold (Tr_{α}) was applied to the proposed damage index values for single-, double-, and triple-damage scenarios based on the damage index values, and the best mother wavelet was selected and considered as the most sensitive mother wavelet to damage identification. The presented values of proposed damage indices in Tables A2–A4 revealed that among the 84 mother wavelets tested from 14 wavelet families, shan1-0.5 was identified as the most effective in detecting damage scenarios using both proposed damage indices *DI_MW* and *DI_SW*. Figures 5–11 illustrate the results achieved by implementing the suggested damage indices with the shan1-0.5 mother wavelet, followed by the implementation of the damage threshold (Tr_α) on all numerical models of the RC beams.

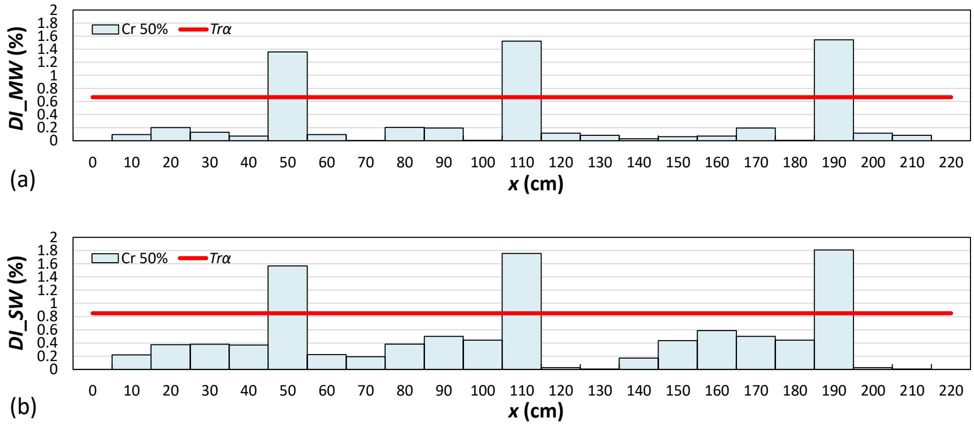

Figure 4. A sample of applying the threshold value (Tr_α) on damage indices: (**a**) *DI_MW* and (**b**) *DI_SW*.

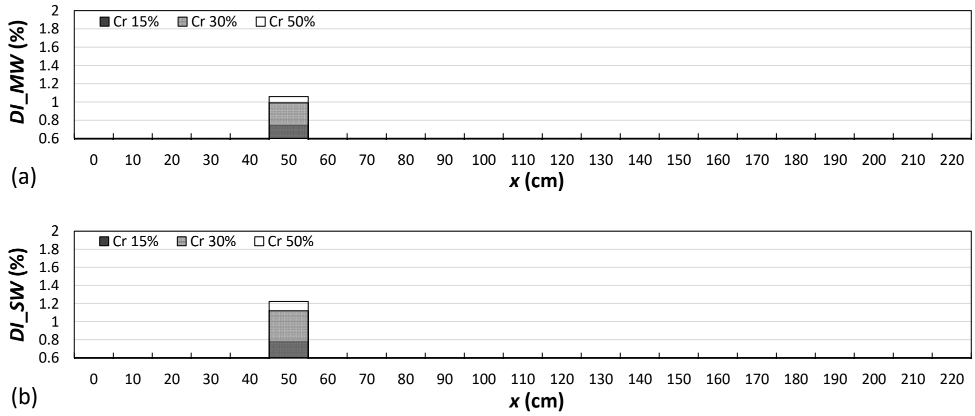

Figure 5. Results of utilizing shan1-0.5 on the numerical models with S_L damage scenario in the proposed damage indices: (**a**) *DI_MW* and (**b**) *DI_SW*.

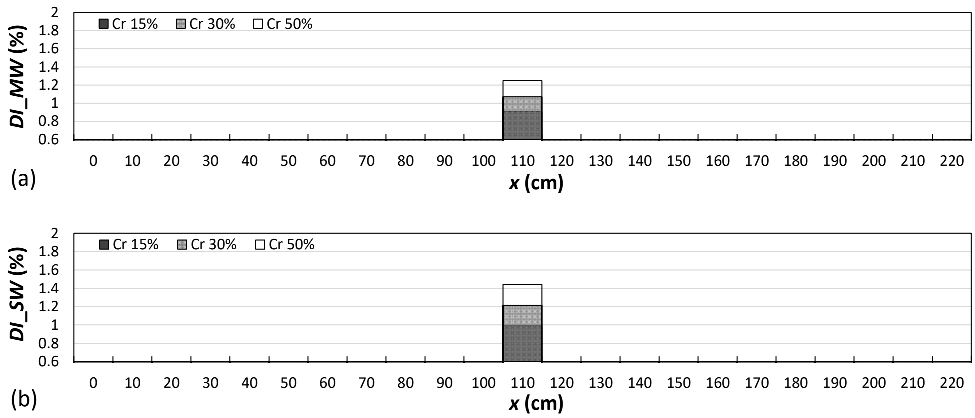

Figure 6. Results of utilizing shan1-0.5 on the numerical models with S_M damage scenario in the proposed damage indices: (**a**) *DI_MW* and (**b**) *DI_SW*.

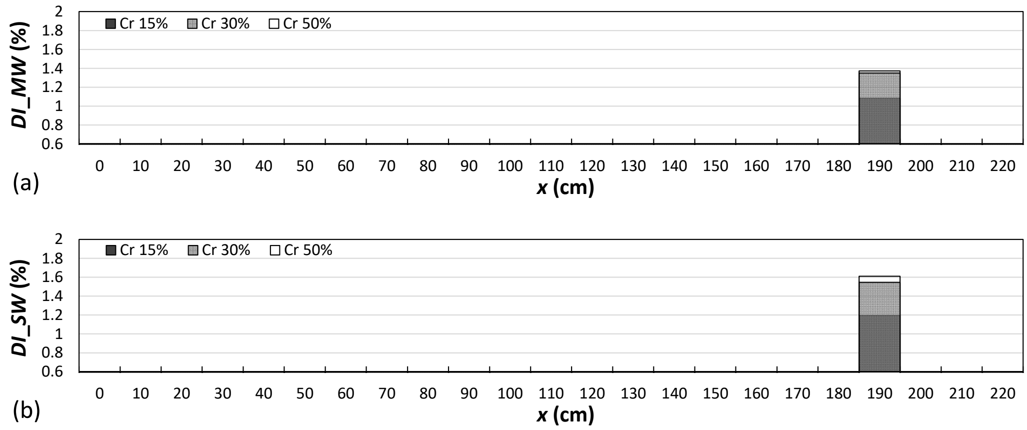

Figure 7. Results of utilizing shan1-0.5 on the numerical models with S_R damage scenario in the proposed damage indices: (**a**) *DI_MW* and (**b**) *DI_SW*.

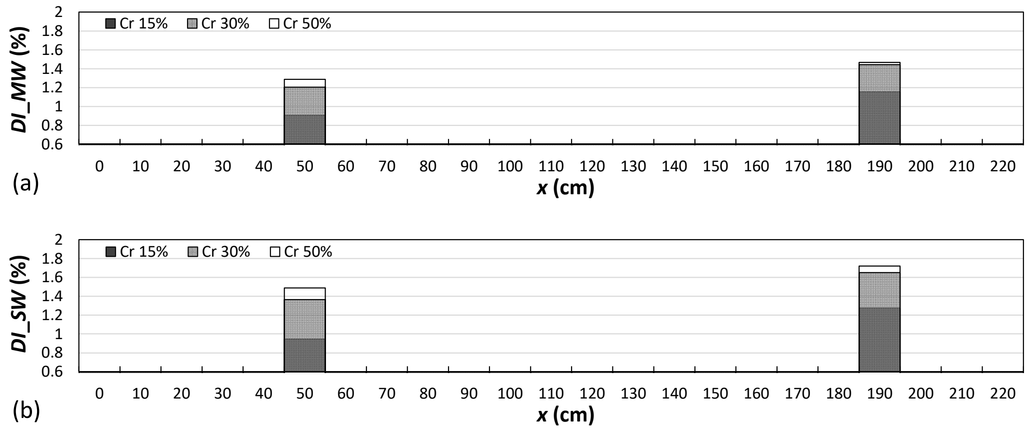

Figure 8. Results of utilizing shan1-0.5 on the numerical models with D_LR damage scenario in the proposed damage indices: (**a**) *DI_MW* and (**b**) *DI_SW*.

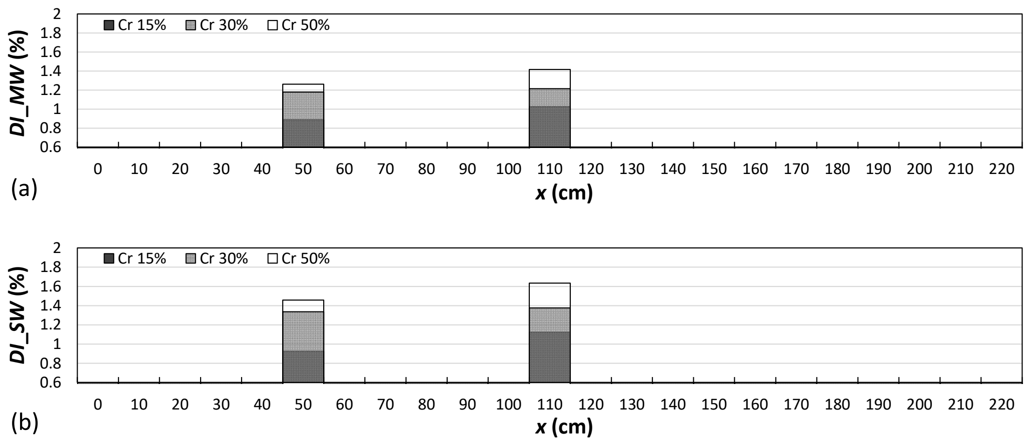

Figure 9. Results of utilizing shan1-0.5 on the numerical models with D_LM damage scenario in the proposed damage indices: (**a**) *DI_MW* and (**b**) *DI_SW*.

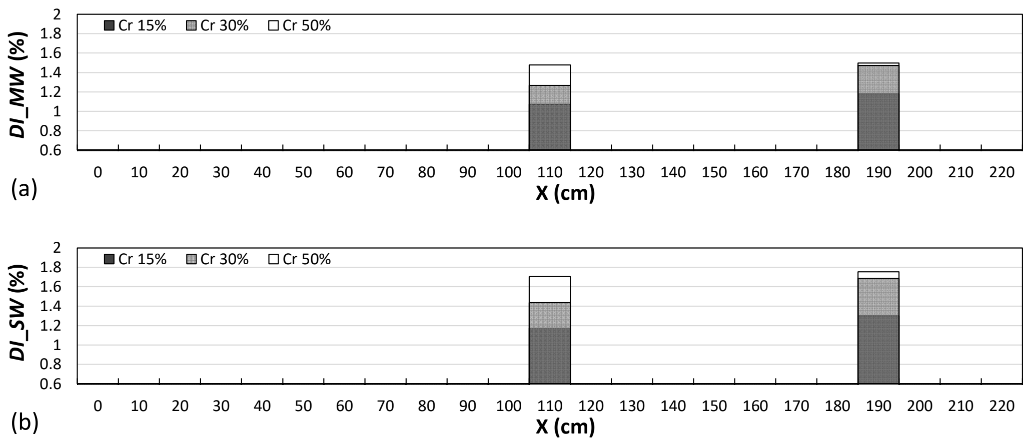

Figure 10. Results of utilizing shan1-0.5 on the numerical models with D_MR damage scenario in the proposed damage indices: (**a**) *DI_MW* and (**b**) *DI_SW*.

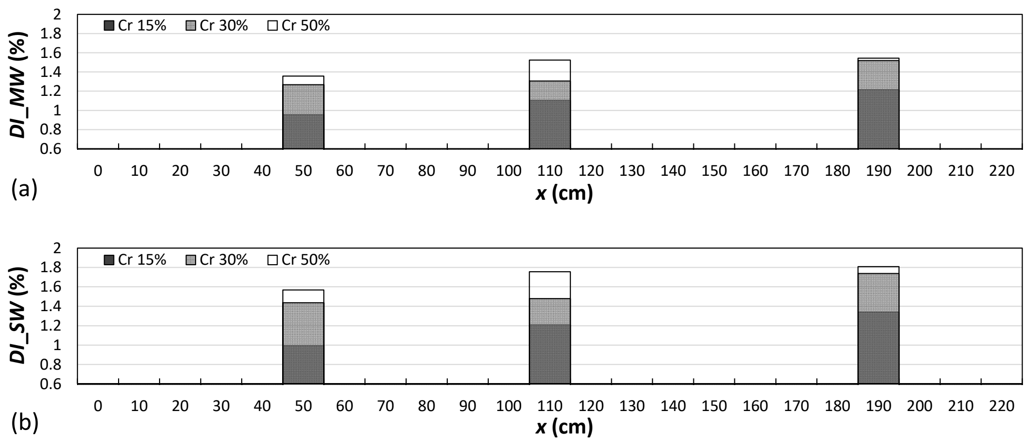

Figure 11. Results of utilizing shan1-0.5 on the numerical models with T_LMR damage scenario in the proposed damage indices: (**a**) *DI_MW* and (**b**) *DI_SW*.

Figures 5–11 demonstrate the results of the damage identification process, where the identified DOFs exceeding the threshold value are considered damaged. By utilizing the specific mother wavelet and the damage threshold, the location and severity of damage can be accurately identified. The incorporation of the damage threshold added an extra layer of accuracy and reliability to the damage identification process, ensuring that only significant DOFs were classified as damaged.

As previously reported in Table 3, the shan1-0.5, shan1-0.1, and fbsp2-1-0.1 mother wavelets from the Shannon and Frequency B-Spline wavelet families showed their effectiveness in identifying damage locations for both proposed damage indices, *DI_MW* and *DI_SW*. Herewith, an analytical comparison was conducted to investigate the results of utilizing the three selected mother wavelets, shan1-0.5, shan1-0.1, and fbsp2-1-0.1, in the proposed damage indices, *DI_MW* and *DI_SW*, for which its outcomes for single-, double-, and triple-damage scenarios were revealed in Figures 12–14, respectively.

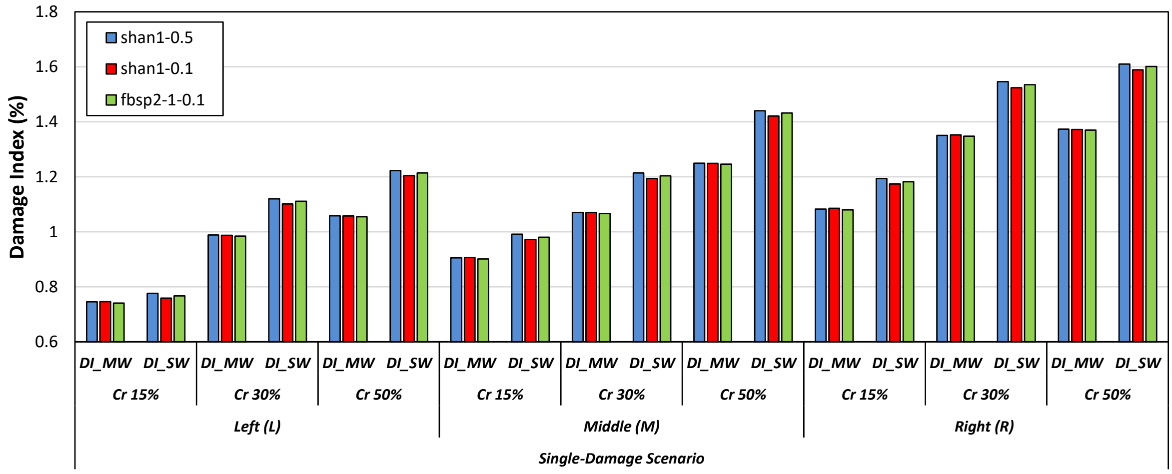

Figure 12. Comparison of the damage severities for the single-damage scenario in the proposed damage indices.

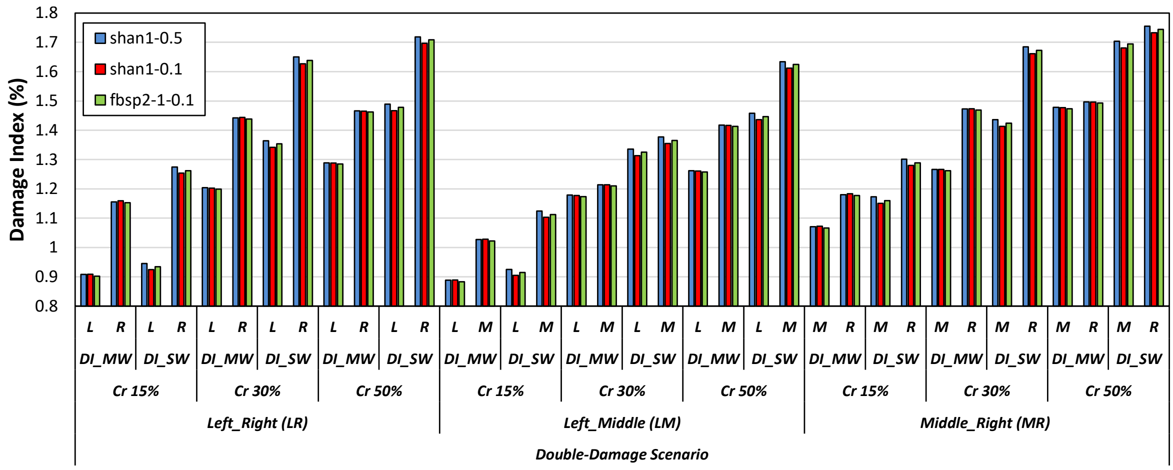

Figure 13. Comparison of the damage severities for the double-damage scenario in the proposed damage indices.

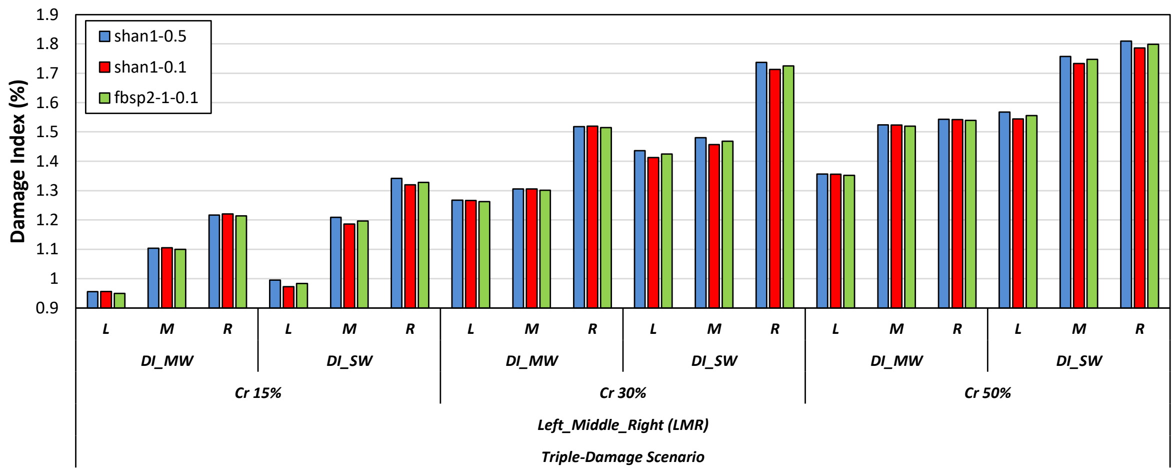

Figure 14. Comparison of the damage severities for the triple-damage scenario in the proposed damage indices.

Figure 12 shows a comparison of the damage severities for a single-damage scenario in the proposed damage indices. The damage scenario considered was single cracks with depth ratios of Cr 15%, Cr 30%, and Cr 50% located at the left (L), middle (M), and right (R) sides of the RC beam. The presented results in Figure 12 show that both damage indices can detect the location of the left, middle, and right cracks, and their values increased as the crack depth of the damage scenarios increases from Cr 15% to Cr 50% which can be considered as a severity detection ability for the proposed indices. Moreover, *DI_SW* using the shan1-0.5 obtained higher values for all damage scenarios compared to *DI_MW* and the other mother wavelets. Furthermore, as the attached sensor location to the RC beam (x = 1900 mm) was near the considered location of the right-side cracks (x = 1600 mm) in comparison to the location of the left-side (x = 500 mm) and middle-side (x = 1100 mm) cracks, near the placement of the sensor with respect to the damage locations, it causes higher values of acceleration, and as a result, the values of the proposed damage indices for the right-side cracks were greater than the corresponding values for the middle and left-sided cracks.

Figure 13 shows the comparison of damage severities for double-damage scenarios using the suggested *DI_MW* and *DI_SW* damage indices. The considered damage scenarios included double cracks with depth ratios of Cr 15%, Cr 30%, and Cr 50% located at the LR, LM, and MR of the RC beam. The results depicted in Figure 13 demonstrate that similar to the single-damage scenario, the shan1-0.5 mother wavelet exhibited the highest sensitivity in detecting double-damage scenarios. It was followed by the shan1-0.1 and fbsp2-1-0.1 mother wavelets.

Additionally, the *DI_SW* damage index exhibited greater differences and higher accuracy compared to the *DI_MW* damage index for all damage scenarios. This observation suggests that the *DI_SW* index is more effective in detecting damage. Moreover, it can be observed that as the crack depth ratios increased from Cr 15% to Cr 30% to Cr 50%, the damage indices values increased as well, suggesting that the proposed damage indices can effectively ascertain the severities of cracks in double-damage scenarios.

Figure 14 presents a comparative analysis of the proposed damage indices in identifying the triple-damage scenario consisting of cracks located simultaneously at the left, middle, and right (LMR) sides of the RC beam, with the same depths of Cr 15%, Cr 30%, and Cr 50%. The analysis was conducted using three different mother wavelets, shan1-0.5, shan1-0.1, and fbsp2-1-0.1, and comparing the results obtained from the *DI_MW* and *DI_SW* damage indices. The results in Figure 14 reveal that both damage indices can successfully detect the damage scenarios, and their values increased in proportion to the crack depths. Moreover, as the same outcome driven from the single- and double-damage scenarios, in the triple-damage scenario, the proposed damage index *DI_SW* using the shan1-0.5 mother wavelet demonstrated higher sensitivity in detecting damage scenarios than the proposed damage index *DI_MW* and other mother wavelets.

Overall, the results of Figures 12–14 show that the proposed damage indices were shown to be effective in identifying single and multiple damage scenarios. The results of this study provide support for the effectiveness of the suggested damage indices in identifying the damage locations as well as describing the severities of damages in reinforced concrete beams modeled in the current study.

5. Conclusions

In summary, this study proposed a methodology, based on wavelet transform, for identifying damages in reinforced concrete beams modeled in the current study using vibration-based damage indices and statistical analysis, including mean and standard deviation to introduce the damage thresholds. The proposed methodology consisted of several steps. First, finite element simulations were conducted using ABAQUS software. These simulations encompassed single-, double-, and triple-damage scenarios, each with three different severities. Next, various wavelet transforms were applied, specifically 14 wavelet families consisting of 84 mother wavelets. Two damage indices were computed based on the acceleration responses of the RC beams. The first index, named *DI_MW*, was derived from the maximal values of detail coefficients obtained from the wavelet transform.

The second index, named *DI_SW*, was calculated as the area under the graph of the detail coefficients of the wavelet transform. In summary, the methodology involved conducting finite element simulations, utilizing multiple wavelet transforms, and computing two distinct damage indices, *DI_MW* and *DI_SW*, based on the acceleration responses of the RC beams. The application of a damage threshold based on statistical data was introduced to enhance the accuracy and reliability of the damage identification process. The following outcomes were obtained in this paper:

- The study's results implied that the use of *DI_SW* showed superior effectiveness in detecting damage across different numerical models compared to *DI_MW*.
- Specific types of mother wavelets, including db2, db6, and db9 from the Daubechies wavelet family, sym2 and sym7 from the Symlets wavelet family, as well as bior2.8 and bior3.1 from the Biorthogonal wavelet family, were found efficient in detecting damage scenarios via the *DI_SW* damage index. Furthermore, it was observed that db10 and fbsp1-1-0.5 were adequate for *DI_MW* to identify the damage scenarios. Some of the mother wavelets from the Shannon and Frequency B-Spline wavelet families, including shan1-0.5, shan1-0.1, and fbsp2-1-0.1, were also effective in both the *DI_MW* and *DI_SW* damage indices.
- Among all the tested mother wavelets, the shan1-0.5 wavelet was found to be particularly effective in detecting damage scenarios using the *DI_SW* damage index.
- As the attached sensor location to the RC beam was near the considered locations of the right-side cracks in comparison to the locations of the left-side and middle-side cracks, the values of the proposed damage indices for the right-side cracks were greater than the corresponding values for the middle and left-side cracks.
- The results showed that both damage indices can detect the location of the left, middle, and right cracks for the single-, double-, and triple-damage scenarios. It was also observed that as the crack depth ratios increased, the damage indices values increased, suggesting that the proposed damage indices could effectively ascertain the severities of cracks in all damage scenarios.

Author Contributions: Conceptualisation, A.S., H.J. and M.R.; methodology, A.S., H.J. and M.R.; software, A.S. and H.J.; validation, H.J. and M.R.; formal analysis, A.S. and H.J.; investigation, A.S., H.J. and M.R.; resources, A.S., H.J., M.R., F.F.M., M.B. and A.J.; data curation, A.S. and H.J.; writing—original draft preparation, A.S., H.J., M.R., F.F.M., M.B. and A.J.; writing—review and editing, A.S., H.J., M.R., F.F.M., M.B. and A.J.; visualisation, A.S. and H.J.; supervision, H.J. and M.R.; project administration, H.J. and M.R.; funding acquisition, M.R. and A.J. All authors have read and agreed to the published version of the manuscript.

Funding: This research received no external funding.

Data Availability Statement: The data presented in this study are available on request from the corresponding author. The data are not publicly available due to privacy restrictions.

Conflicts of Interest: The authors declare no conflict of interest.

Appendix A

This Appendix lists the characteristics of the 14 wavelet families and their 84 related mother wavelets applied to the numerical models of the selected RC beams. These characteristics are described by the waveinfo function in MATLAB® and further information on each family can be found in the references listed in Table A1. Tables A2–A4 report the results of applying proposed damage indices on the numerical models of RC beams.

Table A1. The applied wavelet families and their corresponding wavelet mothers in the current study.

Family	Mother Wavelet	General Characteristics	Order N		Orthogonal	Biorthogonal	Compact Support	DWT	CWT	Support Width	Effective Support	Filters Length	Regularity	Symmetry	Number of Vanishing Moments	Number of Vanishing Moments
			Nr	Nd												
Daubechies [52]	db1 = haar db2 db3 db4 db5 db6 db7 db8 db9 db10	Compactly supported wavelets with extremal phase and the highest number of vanishing moments for a given support width. Associated scaling filters are minimum-phase filters.	N strictly positive integer		✓	✓	✓	✓	✓	$2N-1$	—	$2N$	About $0.2N$ for large N	far from	N	—
Symlets [52]	sym2 sym3 sym4 sym5 sym6 sym7 sym8	Compactly supported wavelets with the least asymmetry and highest number of vanishing moments for a given support width. Associated scaling filters are near linear-phase filters.	$N = 2, 3, \ldots$		✓	✓	✓	✓	✓	$2N-1$	—	$2N$	—	near from	N	—

Table A1. *Cont.*

Family	Mother Wavelet	General Characteristics	Order N Nr	Order N Nd	Orthogonal	Biorthogonal	Compact Support	DWT	CWT	Support Width	Effective Support	Filters Length	Regularity	Symmetry	Number of Vanishing Moments	Number of Vanishing Moments
Coiflets [52]	coif1	Compactly supported wavelets with the highest number of vanishing moments for both phi and psi for a given support width.	$N = 1, 2, \ldots, 5$		✓	✓	✓	✓	✓	$6N-1$	—	$6N$	—	near from	$2N$	$2N-1$
	coif2															
	coif3															
	coif4															
	coif5															
Biorthogonal [52]	bior1.1	Compactly supported biorthogonal spline wavelets for which symmetry and exact reconstruction are possible with finite impulse response (FIR) filters (in orthogonal case it is impossible except for Haar).	1	1, 3, 5	x	✓	✓	✓	✓	$2Nr+1$ for reconstruction? $2Nd+1$ for decomposition	—	max(2Nr,2Nd)+2	$Nr-1$ and $Nr-2$ at the knots	✓	Nr	—
	bior1.3															
	bior1.5															
	bior2.2		2	2, 4, 6, 8												
	bior2.4															
	bior2.6															
	bior2.8															
	bior3.1		3	1, 3, 5, 7, 9												
	bior3.3															
	bior3.5															
	bior3.7															
	bior3.9															
	bior4.4		4	4												
	bior5.5		5	5												
	bior6.8		6	8												

Table A1. *Cont.*

Family	Mother Wavelet	General Characteristics	Order N		Orthogonal	Biorthogonal	Compact Support	DWT	CWT	Support Width	Effective Support	Filters Length	Regularity	Symmetry	Number of Vanishing Moments	Number of Vanishing Moments
			Nr	Nd												
Reverse Biorthogonal [48]	rbio1.1	Compactly supported biorthogonal spline wavelets for which symmetry and exact reconstruction are possible with finite impulse response (FIR) filters (in orthogonal case it is impossible except for Haar).	1	1, 3, 5	x	✓	✓	✓	✓	$2Nd+1$ for reconstruction? $2Nr+1$ for decomposition?	—	max($2Nd$,$2Nr$)+2	$N-1$ and $Nd-2$ at the knots	✓	Nd	—
	rbio1.3															
	rbio1.5															
	rbio2.2		2	2, 4, 6, 8												
	rbio2.4															
	rbio2.6															
	rbio2.8															
	rbio3.1		3	1, 3, 5, 7, 9												
	rbio3.3															
	rbio3.5															
	rbio3.7															
	rbio3.9															
	rbio4.4		4	4												
	rbio5.5		5	5												
	rbio6.8		6	8												
Meyer [52]	meyr	Infinitely regular orthogonal wavelet.	—	—	✓	✓	x	Possible but without FWT	✓	Infinite	[−8, 8]	—	Indefinitely derivable	✓	—	—
Disc.Meyer [52]	dmey	Finite impulse response (FIR)-based approximation of the Meyer wavelet.	—	—	✓	✓	✓	✓	✓	—	—	—	—	—	—	—

Table A1. *Cont.*

Family	Mother Wavelet	General Characteristics	Order N		Orthogonal	Biorthogonal	Compact Support	DWT	CWT	Support Width	Effective Support	Filters Length	Regularity	Symmetry	Number of Vanishing Moments	Number of Vanishing Moments
			Nr	Nd												
Gaussian [52]	gaus1 gaus2 gaus3 gaus4 gaus5 gaus6 gaus7 gaus8	Derivatives of the Gaussian probability density function $f(x) = C_n e^{-x^2}$ where C_n is a constant.	—	—	x	x	x	x	✓	Infinite	$[-5, 5]$	—	—	n even = symmetry n odd = anti-symmetry	—	—
Mexican hat [52]	mexh	The second derivative of the Gaussian probability density function $mexh(x) = -\frac{2\sqrt{3}e^{-\frac{x^2}{2}}(x^2-1)}{3\pi^{1/4}}$	—	—	x	x	x	x	✓	Infinite	$[-5, 5]$	—	—	✓	—	—
Morlet [53]	morl	$\mathrm{morl}(x) = \cos(5x)e^{\frac{-x^2}{2}}$	—	—	x	x	x	x	✓	Infinite	$[-4, 4]$	—	—	✓	—	—
Complex Gaussian	cgau1 cgau2 cgau3 cgau4 cgau5	Derivatives of the complex Gaussian function: $f(x) = C_n e^{-xi} e^{-x^2}$ where C_n is a constant.	—	—	x	x	x	x	✓	Infinite	—	—	—	n even = symmetry n odd = anti-symmetry	—	—

Table A1. *Cont.*

Family	Mother Wavelet	General Characteristics	Order N		Orthogonal	Biorthogonal	Compact Support	DWT	CWT	Support Width	Effective Support	Filters Length	Regularity	Symmetry	Number of Vanishing Moments	Number of Vanishing Moments
			Nr	Nd												
Shannon [49]	shan1-1.5 shan1-1 shan1-0.5 shan1-0.1 shan2-3	$shan(x) = \frac{\sin(\pi f_b x) e^{2\pi f_c x i}}{\sqrt{f_b} x \pi}$ where f_b is a bandwidth parameter and f_c is a wavelet center frequency.	—	—	x	x	x	x	✓	Infinite	—	—	—	—	—	—
Frequency B-Spline [53]	fbsp1-1-1.5 fbsp1-1-1 fbsp1-1-0.5 fbsp2-1-1 fbsp2-1-0.5 fbsp2-1-0.1	$fbsp(x) = \sqrt{f_b} e^{2\pi f_c x i} \left(\frac{M \sin\left(\frac{\pi f_b x}{M}\right)}{f_b x \pi} \right)^M$ where M is an integer-order parameter (>=1), f_b is a bandwidth parameter, and f_c is a wavelet center frequency.	—	—	x	x	x	x	✓	Infinite	—	—	—	—	—	—
Complex Morlet [54]	cmor1-1.5 cmor1-1 cmor1-0.5 cmor1-0.1	$cmor(x) = \frac{e^{-\frac{x^2}{f_b}} e^{2\pi f_c x_i}}{\sqrt{\pi f_b}}$ where f_b is a bandwidth parameter and f_c is a wavelet center frequency.	—	—	x	x	x	x	✓	Infinite	—	—	—	—	—	—

Table A2. The values of proposed damage indices for single-damage scenarios.

		Single-Damage Scenario																	
		Left (S_L)						**Middle (S_M)**						**Right (S_R)**					
		Cr 15%		**Cr 30%**		**Cr 50%**		**Cr 15%**		**Cr 30%**		**Cr 50%**		**Cr 15%**		**Cr 30%**		**Cr 50%**	
Wavelet Families		*DI_MW*	*DI_SW*	*DI_MW*	*DI_SW*	*DI_MW*	*DI_SW*	*DI_MW*	*DI_SW*	*DI_MW*	*DI_SW*	*DI_MW*	*DI_SW*	*DI_MW*	*DI_SW*	*DI_MW*	*DI_SW*	*DI_MW*	*DI_SW*
db	db1 = haar				1.082		1.208		0.995		1.204		1.406		1.247		1.553		1.6
	db2		1.02		1.139		1.227		1.17		1.272		1.378		1.428		1.563		1.548
	db3																		
	db4				0.859		0.959		0.818		0.965		1.11		1.033		1.242		1.265
	db5				1.047		1.158		0.952		1.153		1.357		1.172		1.479		1.528
	db6		0.799		0.961		1.035		0.958		1.06		1.183	0.6565	1.158		1.317		1.326
	db7																		
	db8												0.639	0.6486			0.731		0.742
	db9		0.798		1.066		1.158		0.996		1.169		1.348		1.213		1.477		1.505
	db10	0.91769		0.7017	0.861	0.7096	0.951	0.9385	0.752	0.8117	0.938	0.7593	1.133	1.1666	0.918	0.9462	1.221	0.7939	1.274
sym	**sym2**		0.868		0.969		1.044		0.995		1.083		1.172		1.215		1.33		1.318
	sym3																		
	sym4												0.599		0.633		0.697		0.69
	sym5				0.874		0.944		0.813		0.947		1.091		0.985		1.211		1.246
	sym6													0.5307					
	sym7		0.86		1.034		1.101		1.028		1.135		1.259	0.5798	1.192	0.5456	1.387		1.405
	sym8	0.49848												0.6389					
coif	coif1	0.51153						0.5297	0.523		0.517		0.516	0.7088	0.688		0.647		0.596
	coif2													0.5888					
	coif3													0.6148					
	coif4																		
	coif5																		
bior	bior1.1																		
	bior1.3	0.54322						0.547						0.734					
	bior1.5	0.54456						0.5528						0.7438					
	bior2.2																0.503		
	bior2.4												0.512		0.625		0.629		0.582
	bior2.6						0.532		0.572		0.573		0.586		0.693		0.7		0.656
	bior2.8		0.539		0.549		0.585		0.628		0.629		0.66		0.719		0.755		0.707
	bior3.1		0.916		1.225		1.328	0.5548	1.142	0.5681	1.34	0.6021	1.539	0.7837	1.373	0.7563	1.686	0.7096	1.722
	bior3.3					0.5611		0.5663		0.5835	0.563	0.6206	0.65	0.7973	0.572	0.776	0.708	0.7307	0.727
	bior3.5					0.5739		0.5765		0.5963		0.6355		0.8094		0.7922	0.577	0.7474	0.592
	bior3.7					0.5856		0.5869		0.6083		0.649		0.8215		0.807	0.536	0.7624	0.55
	bior3.9					0.5969		0.5977		0.6202		0.6618		0.834		0.8212		0.7763	0.531
	bior4.4													0.6316					
	bior5.5													0.5574					
	bior6.8																		

Table A2. *Cont.*

		Single-Damage Scenario																	
		Left (S_L)						**Middle (S_M)**						**Right (S_R)**					
		Cr 15%		**Cr 30%**		**Cr 50%**		**Cr 15%**		**Cr 30%**		**Cr 50%**		**Cr 15%**		**Cr 30%**		**Cr 50%**	
Wavelet Families		*DI_MW*	*DI_SW*	*DI_MW*	*DI_SW*	*DI_MW*	*DI_SW*	*DI_MW*	*DI_SW*	*DI_MW*	*DI_SW*	*DI_MW*	*DI_SW*	*DI_MW*	*DI_SW*	*DI_MW*	*DI_SW*	*DI_MW*	*DI_SW*
rbio	rbio1.1																		
	rbio1.3							0.5589		0.5721		0.6063		0.7887		0.7611		0.714	
	rbio1.5													0.7377		0.6792		0.6242	
	rbio2.2																		
	rbio2.4													0.5104					
	rbio2.6																		
	rbio2.8													0.4922					
	rbio3.1											0.7185		0.8785		0.8755	0.562	0.8373	0.574
	rbio3.3																		
	rbio3.5					0.7114				0.7127		0.8014		0.8944		0.9814		0.9683	
	rbio3.7													0.7741		0.7179		0.6628	
	rbio3.9													0.7303		0.631		0.5623	
	rbio4.4													0.5717					
	rbio5.5																		
	rbio6.8																		
meyr	meyr																		
dmey	dmey																		
gaus	gaus1				0.885		0.972		0.803		0.97		1.137		0.981		1.237		1.277
	gaus2																		
	gaus3																		
	gaus4																		
	gaus5																		
	gaus6													0.5374					
	gaus7																		
	gaus8																		
mexh	mexh						0.517				0.522		0.608		0.567		0.678		0.683
morl	morl																		
cgau	cgau1							0.8087		0.7862		0.7959	0.633		0.562		0.694		0.714
	cgau2																		
	cgau3																		
	cgau4	0.53962						0.5468						0.7328					
	cgau5																		
shan	shan1-1.5																		
	shan1-1																		
	shan1-0.5	0.7452	0.776	0.9887	1.12	1.0583	1.223	0.9053	0.991	1.0705	1.214	1.2497	1.441	1.0826	1.194	1.3511	1.546	1.3734	1.61
	shan1-0.1	0.74581	0.759	0.9874	1.102	1.0574	1.204	0.9064	0.973	1.0705	1.194	1.249	1.421	1.0859	1.174	1.3522	1.524	1.3724	1.59
	shan2-3																		
fbsp	fbsp1-1-1.5																		
	fbsp1-1-1																		
	fbsp1-1-0.5	0.7452		0.9887		1.0583	0.586	0.9053		1.0705	0.582	1.2497	0.691	1.0826	0.573	1.3511	0.741	1.3734	0.772
	fbsp2-1-1																		
	fbsp2-1-0.5																		
	fbsp2-1-0.1	0.74073	0.767	0.9844	1.111	1.0548	1.214	0.9016	0.981	1.0667	1.204	1.2459	1.432	1.0801	1.182	1.3478	1.535	1.3699	1.601
cmor	cmor1-1.5																		
	cmor1-1															0.5409			
	cmor1-0.5			0.806		0.9174				0.8849		1.1165		0.8344		1.1819		1.2502	
	cmor1-0.1			0.9941		1.1065	0.725	0.8188		1.0732	0.715	1.3302	0.866	0.991		1.3994	0.904	1.4888	0.954

Table A3. The values of proposed damage indices for double-damage scenarios.

		Double-Damage Scenario																																			
		Left_Right (D_LR)												**Left_Middle (D_LM)**												**Middle_Right (D_MR)**											
		Cr 15%				**Cr 30%**				**Cr 50%**				**Cr 15%**				**Cr 30%**				**Cr 50%**				**Cr 15%**				**Cr 30%**				**Cr 50%**			
Wavelet		*DI_MW*		*DI_SW*		*DI_MW*		*DI_SW*		*DI_MW*		*DI_SW*		*DI_MW*		*DI_SW*		*DI_MW*		*DI_SW*		*DI_MW*		*DI_SW*		*DI_MW*		*DI_SW*		*DI_MW*		*DI_SW*		*DI_MW*		*DI_SW*	
Families		**L**	**R**	**L**	**R**	**L**	**R**	**L**	**R**	**L**	**R**	**L**	**R**	**L**	**M**	**L**	**M**	**L**	**M**	**L**	**M**	**L**	**M**	**L**	**M**	**M**	**R**	**M**	**R**	**M**	**R**	**M**	**R**	**M**	**R**	**M**	**R**
db	db1 = haar			0.91	1.331			1.318	1.658			1.471	1.708			0.89	1.129			1.29	1.365			1.44	1.595			1.177	1.359			1.424	1.693			1.664	1.744
	db2			1.243	1.525			1.388	1.668			1.495	1.653			1.217	1.327			1.358	1.443			1.463	1.562			1.384	1.557			1.505	1.703			1.63	1.688
	db3																																				
	db4			0.755	1.103			1.046	1.326			1.169	1.35			0.74	0.928			1.024	1.094			1.144	1.259			0.967	1.126			1.141	1.354			1.313	1.379
	db5			0.896	1.251			1.276	1.578			1.411	1.631			0.877	1.079			1.249	1.308			1.381	1.539			1.126	1.277			1.364	1.611			1.605	1.665
	db6			0.974	1.237			1.171	1.406			1.261	1.415			0.953	1.086			1.146	1.202			1.234	1.341			1.133	1.263			1.254	1.436			1.399	1.445

Table A3. *Cont.*

		Double-Damage Scenario																																			
		Left_Right (D_LR)												**Left_Middle (D_LM)**												**Middle_Right (D_MR)**											
		Cr 15%				**Cr 30%**				**Cr 50%**				**Cr 15%**				**Cr 30%**				**Cr 50%**				**Cr 15%**				**Cr 30%**				**Cr 50%**			
Wavelet		*DI_MW*		*DI_SW*		*DI_MW*		*DI_SW*		*DI_MW*		*DI_SW*		*DI_MW*		*DI_SW*		*DI_MW*		*DI_SW*		*DI_MW*		*DI_SW*		*DI_MW*		*DI_SW*		*DI_MW*		*DI_SW*		*DI_MW*		*DI_SW*	
Families		**L**	**R**	**L**	**R**	**L**	**R**	**L**	**R**	**L**	**R**	**L**	**R**	**L**	**M**	**L**	**M**	**L**	**M**	**L**	**M**	**L**	**M**	**L**	**M**	**M**	**R**	**M**	**R**	**M**	**R**	**M**	**R**	**M**	**R**	**M**	**R**
	db7																																				
	db8	0.5674	0.6923									0.67	0.792	0.5554	0.5553									0.655	0.725	0.5792	0.7069					0.658	0.797			0.756	0.809
	db9			0.972	1.294			1.298	1.577			1.41	1.607			0.952	1.13			1.27	1.325			1.38	1.529			1.178	1.322			1.382	1.61			1.594	1.641
	db10	1.1177	1.2452			0.8547	1.01	1.049	1.303	0.8642	0.8474	1.158	1.36	1.0942	1.0644			0.8367	0.9206	1.027	1.063	0.846	0.8612	1.133	1.285	1.1102	1.2714	0.889	1.001	0.9602	1.0312	1.109	1.33	0.8982	0.8652	1.34	1.389
sym	**sym2**			1.058	1.297			1.181	1.42			1.272	1.406			1.035	1.129			1.156	1.228			1.245	1.33			1.177	1.325			1.281	1.45			1.387	1.436
	sym3																																				

Table A3. *Cont.*

		Double-Damage Scenario																																			
		Left_Right (D_LR)												**Left_Middle (D_LM)**												**Middle_Right (D_MR)**											
		Cr 15%				**Cr 30%**				**Cr 50%**				**Cr 15%**				**Cr 30%**				**Cr 50%**				**Cr 15%**				**Cr 30%**				**Cr 50%**			
Wavelet		*DI_MW*		*DI_SW*		*DI_MW*		*DI_SW*		*DI_MW*		*DI_SW*		*DI_MW*		*DI_SW*		*DI_MW*		*DI_SW*		*DI_MW*		*DI_SW*		*DI_MW*		*DI_SW*		*DI_MW*		*DI_SW*		*DI_MW*		*DI_SW*	
Families		**L**	**R**	**L**	**R**	**L**	**R**	**L**	**R**	**L**	**R**	**L**	**R**	**L**	**M**	**L**	**M**	**L**	**M**	**L**	**M**	**L**	**M**	**L**	**M**	**M**	**R**	**M**	**R**	**M**	**R**	**M**	**R**	**M**	**R**	**M**	**R**
	sym4											0.651	0.737											0.637	0.68							0.65	0.76			0.709	0.752
	sym5			0.812	1.051			1.065	1.293			1.15	1.33			0.795	0.922			1.042	1.074			1.125	1.237			0.962	1.073			1.121	1.32			1.29	1.358
	sym6																																				
	sym7			1.047	1.272			1.26	1.481			1.341	1.5			1.025	1.166			1.233	1.288			1.313	1.428			1.216	1.299			1.343	1.512			1.49	1.531
	sym8	0.6071	0.6819											0.5943	0.5559											0.5798	0.6963										
coif	coif1	0.623	0.7566									0.583	0.636	0.6099	0.6007									0.571	0.586	0.6266	0.7725	0.619	0.75			0.612	0.705			0.611	0.649

Table A3. *Cont.*

		Double-Damage Scenario																																			
		Left_Right (D_LR)												**Left_Middle (D_LM)**												**Middle_Right (D_MR)**											
		Cr 15%				**Cr 30%**				**Cr 50%**				**Cr 15%**				**Cr 30%**				**Cr 50%**				**Cr 15%**				**Cr 30%**				**Cr 50%**			
Wavelet Families		*DI_MW*		*DI_SW*		*DI_MW*		*DI_SW*		*DI_MW*		*DI_SW*		*DI_MW*		*DI_SW*		*DI_MW*		*DI_SW*		*DI_MW*		*DI_SW*		*DI_MW*		*DI_SW*		*DI_MW*		*DI_SW*		*DI_MW*		*DI_SW*	
		L	**R**	**L**	**R**	**L**	**R**	**L**	**R**	**L**	**R**	**L**	**R**	**L**	**M**	**L**	**M**	**L**	**M**	**L**	**M**	**L**	**M**	**L**	**M**	**M**	**R**	**M**	**R**	**M**	**R**	**M**	**R**	**M**	**R**	**M**	**R**
	coif2	0.5484	0.6285																							0.5238	0.6418										
	coif3	0.5888	0.6563											0.5764	0.5332											0.5561	0.6701										
	coif4																																				
	coif5																																				
bior	bior1.1																																				
bior	bior1.3	0.6616	0.7835											0.6477	0.6203											0.647	0.8										

Table A3. *Cont.*

		Double-Damage Scenario																																			
		Left_Right (D_LR)												**Left_Middle (D_LM)**												**Middle_Right (D_MR)**											
		Cr 15%				**Cr 30%**				**Cr 50%**				**Cr 15%**				**Cr 30%**				**Cr 50%**				**Cr 15%**				**Cr 30%**				**Cr 50%**			
Wavelet Families		*DI_MW*		*DI_SW*		*DI_MW*		*DI_SW*		*DI_MW*		*DI_SW*		*DI_MW*		*DI_SW*		*DI_MW*		*DI_SW*		*DI_MW*		*DI_SW*		*DI_MW*		*DI_SW*		*DI_MW*		*DI_SW*		*DI_MW*		*DI_SW*	
		L	**R**	**L**	**R**	**L**	**R**	**L**	**R**	**L**	**R**	**L**	**R**	**L**	**M**	**L**	**M**	**L**	**M**	**L**	**M**	**L**	**M**	**L**	**M**	**M**	**R**	**M**	**R**	**M**	**R**	**M**	**R**	**M**	**R**	**M**	**R**
	bior1.5	0.6632	0.7939											0.6493	0.627											0.654	0.8106										
	bior2.2																																			0.53	0.521
	bior2.4											0.567	0.621											0.555	0.581			0.592	0.681			0.593	0.685			0.606	0.635
	bior2.6			0.58	0.74			0.592	0.747			0.648	0.7			0.568	0.648			0.579	0.65			0.635	0.665			0.676	0.756			0.677	0.763			0.694	0.714
	bior2.8			0.656	0.767			0.668	0.806			0.712	0.755			0.642	0.712			0.654	0.714			0.697	0.748			0.742	0.783			0.745	0.823			0.78	0.771
	bior3.1			1.116	1.465			1.492	1.8	0.6642	0.7575	1.618	1.838			1.093	1.295			1.461	1.52	0.6502	0.6829	1.584	1.746	0.6563	0.8542	1.351	1.496	0.672	0.8243	1.585	1.838	0.7123	0.7734	1.821	1.876

Table A3. *Cont.*

		Double-Damage Scenario																																			
		Left_Right (D_LR)												**Left_Middle (D_LM)**												**Middle_Right (D_MR)**											
		Cr 15%				**Cr 30%**				**Cr 50%**				**Cr 15%**				**Cr 30%**				**Cr 50%**				**Cr 15%**				**Cr 30%**				**Cr 50%**			
Wavelet Families		*DI_MW*		*DI_SW*		*DI_MW*		*DI_SW*		*DI_MW*		*DI_SW*		*DI_MW*		*DI_SW*		*DI_MW*		*DI_SW*		*DI_MW*		*DI_SW*		*DI_MW*		*DI_SW*		*DI_MW*		*DI_SW*		*DI_MW*		*DI_SW*	
		L	**R**	**L**	**R**	**L**	**R**	**L**	**R**	**L**	**R**	**L**	**R**	**L**	**M**	**L**	**M**	**L**	**M**	**L**	**M**	**L**	**M**	**L**	**M**	**M**	**R**	**M**	**R**	**M**	**R**	**M**	**R**	**M**	**R**	**M**	**R**
	bior3.3							0.631	0.756	0.6833	0.7799	0.68	0.776							0.618	0.638	0.669	0.7039	0.666	0.737	0.6699	0.8689			0.6902	0.8458	0.666	0.772	0.7341	0.7963	0.769	0.792
	bior3.5									0.699	0.7978											0.6842	0.7207			0.682	0.8822			0.7054	0.8634			0.7517	0.8146	0.626	0.645
	bior3.7					0.5956	0.8614			0.7133	0.8138							0.5831	0.6899			0.6983	0.736			0.6942	0.8954			0.7196	0.8795			0.7677	0.8309	0.582	0.6
	bior3.9					0.609	0.8766			0.727	0.8287							0.5962	0.7034			0.7117	0.7506			0.707	0.9089			0.7336	0.895			0.7829	0.8461	0.562	0.579
	bior4.4	0.5912	0.6741											0.5787	0.5401											0.5633	0.6883										
	bior5.5	0.5442	0.595																																		

Table A3. *Cont.*

		Double-Damage Scenario																																			
		Left_Right (D_LR)												**Left_Middle (D_LM)**												**Middle_Right (D_MR)**											
		Cr 15%				**Cr 30%**				**Cr 50%**				**Cr 15%**				**Cr 30%**				**Cr 50%**				**Cr 15%**				**Cr 30%**				**Cr 50%**			
Wavelet		*DI_MW*		*DI_SW*		*DI_MW*		*DI_SW*		*DI_MW*		*DI_SW*		*DI_MW*		*DI_SW*		*DI_MW*		*DI_SW*		*DI_MW*		*DI_SW*		*DI_MW*		*DI_SW*		*DI_MW*		*DI_SW*		*DI_MW*		*DI_SW*	
Families		**L**	**R**	**L**	**R**	**L**	**R**	**L**	**R**	**L**	**R**	**L**	**R**	**L**	**M**	**L**	**M**	**L**	**M**	**L**	**M**	**L**	**M**	**L**	**M**	**M**	**R**	**M**	**R**	**M**	**R**	**M**	**R**	**M**	**R**	**M**	**R**
	bior6.8																																				
rbio	rbio1.1																																				
	rbio1.3									0.6687	0.7621											0.6546	0.6876			0.6612	0.8596			0.6767	0.8295			0.7172	0.7782		
	rbio1.5									0.5886	0.6662											0.5762	0.5991			0.6098	0.804			0.6021	0.7403			0.6249	0.6803		
	rbio2.2																																				
	rbio2.4																																				

Table A3. *Cont.*

Wavelet Families	Double-Damage Scenario																																			
	Left_Right (D_LR)												Left_Middle (D_LM)												Middle_Right (D_MR)											
	Cr 15%				Cr 30%				Cr 50%				Cr 15%				Cr 30%				Cr 50%				Cr 15%				Cr 30%				Cr 50%			
	DI_MW		*DI_SW*		*DI_MW*		*DI_SW*		*DI_MW*		*DI_SW*		*DI_MW*		*DI_SW*		*DI_MW*		*DI_SW*		*DI_MW*		*DI_SW*		*DI_MW*		*DI_SW*		*DI_MW*		*DI_SW*		*DI_MW*		*DI_SW*	
	L	**R**	**L**	**R**	**L**	**R**	**L**	**R**	**L**	**R**	**L**	**R**	**L**	**M**	**L**	**M**	**L**	**M**	**L**	**M**	**L**	**M**	**L**	**M**	**M**	**R**	**M**	**R**	**M**	**R**	**M**	**R**	**M**	**R**	**M**	**R**
rbio2.6																																				
rbio2.8	0.5165	0.5254																																		
rbio3.1									0.784	0.8937											0.7675	0.8149			0.7525	0.9574			0.785	0.9542			0.85	0.9125	0.607	0.625
rbio3.3																																				
rbio3.5					0.6904	1.0475			0.8665	1.0336							0.6759	0.8083			0.8482	0.9089			0.7306	0.9748			0.843	1.0696			0.948	1.0553		
rbio3.7									0.6142	0.7074											0.6012	0.6218			0.621	0.8437			0.6232	0.7825			0.6485	0.7223		

Table A3. *Cont.*

		Double-Damage Scenario																							
		Left_Right (D_LR)												**Left_Middle (D_LM)**												**Middle_Right (D_MR)**											
		Cr 15%				**Cr 30%**				**Cr 50%**				**Cr 15%**				**Cr 30%**				**Cr 50%**				**Cr 15%**				**Cr 30%**				**Cr 50%**			
Wavelet Families		*DI_MW*		*DI_SW*		*DI_MW*		*DI_SW*		*DI_MW*		*DI_SW*		*DI_MW*		*DI_SW*		*DI_MW*		*DI_SW*		*DI_MW*		*DI_SW*		*DI_MW*		*DI_SW*		*DI_MW*		*DI_SW*		*DI_MW*		*DI_SW*	
		L	**R**	**L**	**R**	**L**	**R**	**L**	**R**	**L**	**R**	**L**	**R**	**L**	**M**	**L**	**M**	**L**	**M**	**L**	**M**	**L**	**M**	**L**	**M**	**M**	**R**	**M**	**R**	**M**	**R**	**M**	**R**	**M**	**R**	**M**	**R**
	rbio3.9																									0.5926	0.7959			0.5576	0.6877			0.558	0.6128		
	rbio4.4	0.5416	0.6103																																		
	rbio5.5																																				
	rbio6.8																																				
meyr	meyr																																				
dmey	dmey																																				

Table A3. *Cont.*

		Double-Damage Scenario																																			
		Left_Right (D_LR)												**Left_Middle (D_LM)**												**Middle_Right (D_MR)**											
		Cr 15%				**Cr 30%**				**Cr 50%**				**Cr 15%**				**Cr 30%**				**Cr 50%**				**Cr 15%**				**Cr 30%**				**Cr 50%**			
Wavelet		*DI_MW*		*DI_SW*		*DI_MW*		*DI_SW*		*DI_MW*		*DI_SW*		*DI_MW*		*DI_SW*		*DI_MW*		*DI_SW*		*DI_MW*		*DI_SW*		*DI_MW*		*DI_SW*		*DI_MW*		*DI_SW*		*DI_MW*		*DI_SW*	
Families		**L**	**R**	**L**	**R**	**L**	**R**	**L**	**R**	**L**	**R**	**L**	**R**	**L**	**M**	**L**	**M**	**L**	**M**	**L**	**M**	**L**	**M**	**L**	**M**	**M**	**R**	**M**	**R**	**M**	**R**	**M**	**R**	**M**	**R**	**M**	**R**
gaus	gaus1			0.761	1.047			1.078	1.32			1.184	1.363			0.745	0.911			1.056	1.1			1.159	1.289			0.95	1.069			1.147	1.348			1.344	1.392
	gaus2																																				
	gaus3																																				
	gaus4																																				
	gaus5																																				
	gaus6																																				

Table A3. *Cont.*

		Double-Damage Scenario																																	
		Left_Right (D_LR)												Left_Middle (D_LM)												Middle_Right (D_MR)											
		Cr 15%				Cr 30%				Cr 50%				Cr 15%				Cr 30%				Cr 50%				Cr 15%				Cr 30%				Cr 50%			
Wavelet		*DI_MW*		*DI_SW*		*DI_MW*		*DI_SW*		*DI_MW*		*DI_SW*		*DI_MW*		*DI_SW*		*DI_MW*		*DI_SW*		*DI_MW*		*DI_SW*		*DI_MW*		*DI_SW*		*DI_MW*		*DI_SW*		*DI_MW*		*DI_SW*	
Families		L	R	L	R	L	R	L	R	L	R	L	R	L	M	L	M	L	M	L	M	L	M	L	M	M	R	M	R	M	R	M	R	M	R	M	R
	gaus7																																				
	gaus8																																				
mexh	mexh							0.567	0.724			0.629	0.729							0.555	0.592			0.616	0.69							0.618	0.739			0.719	0.745
morl	morl																																				
cgau	cgau1							0.605	0.741			0.664	0.763							0.592	0.619			0.65	0.718							0.646	0.756			0.748	0.779
	cgau2																																				

Table A3. *Cont.*

		Double-Damage Scenario																																			
		Left_Right (D_LR)												Left_Middle (D_LM)												Middle_Right (D_MR)											
		Cr 15%				Cr 30%				Cr 50%				Cr 15%				Cr 30%				Cr 50%				Cr 15%				Cr 30%				Cr 50%			
Wavelet		*DI_MW*		*DI_SW*		*DI_MW*		*DI_SW*		*DI_MW*		*DI_SW*		*DI_MW*		*DI_SW*		*DI_MW*		*DI_SW*		*DI_MW*		*DI_SW*		*DI_MW*		*DI_SW*		*DI_MW*		*DI_SW*		*DI_MW*		*DI_SW*	
Families		**L**	**R**	**L**	**R**	**L**	**R**	**L**	**R**	**L**	**R**	**L**	**R**	**L**	**M**	**L**	**M**	**L**	**M**	**L**	**M**	**L**	**M**	**L**	**M**	**M**	**R**	**M**	**R**	**M**	**R**	**M**	**R**	**M**	**R**	**M**	**R**
	cgau3																																				
	cgau4	0.6572	0.7822											0.6434	0.6201											0.6468	0.7987										
	cgau5																																				
shan	shan1-1.5																																				
	shan1-1																																				
	shan1-0.5	0.9076	1.1556	0.945	1.275	1.2042	1.4421	1.364	1.65	1.289	1.466	1.489	1.719	0.8885	1.0267	0.925	1.124	1.1789	1.2141	1.336	1.377	1.2618	1.4174	1.458	1.634	1.0709	1.1799	1.173	1.302	1.2663	1.4725	1.436	1.685	1.4784	1.4969	1.704	1.755

Table A3. *Cont.*

		Double-Damage Scenario																																			
		Left_Right (D_LR)												**Left_Middle (D_LM)**												**Middle_Right (D_MR)**											
		Cr 15%				**Cr 30%**				**Cr 50%**				**Cr 15%**				**Cr 30%**				**Cr 50%**				**Cr 15%**				**Cr 30%**				**Cr 50%**			
Wavelet Families		*DI_MW*		*DI_SW*		*DI_MW*		*DI_SW*		*DI_MW*		*DI_SW*		*DI_MW*		*DI_SW*		*DI_MW*		*DI_SW*		*DI_MW*		*DI_SW*		*DI_MW*		*DI_SW*		*DI_MW*		*DI_SW*		*DI_MW*		*DI_SW*	
		L	**R**	**L**	**R**	**L**	**R**	**L**	**R**	**L**	**R**	**L**	**R**	**L**	**M**	**L**	**M**	**L**	**M**	**L**	**M**	**L**	**M**	**L**	**M**	**M**	**R**	**M**	**R**	**M**	**R**	**M**	**R**	**M**	**R**	**M**	**R**
	shan1-0.1	0.9084	1.1591	0.924	1.254	1.2026	1.4434	1.342	1.627	1.2879	1.4649	1.467	1.697	0.8892	1.028	0.905	1.103	1.1772	1.2141	1.314	1.355	1.2608	1.4165	1.436	1.612	1.0722	1.1835	1.151	1.28	1.2663	1.4738	1.413	1.661	1.4774	1.4957	1.681	1.732
	shan2-3																																				
fbsp	fbsp1-1-1.5																																				
	fbsp1-1-1																																				
	fbsp1-1-0.5	0.9076	1.1556			1.2042	1.4421	0.654	0.791	1.289	1.466	0.714	0.824	0.8885	1.0267			1.1789	1.2141	0.641	0.66	1.2618	1.4174	0.699	0.784	1.0709	1.1799			1.2663	1.4725	0.689	0.808	1.4784	1.4969	0.817	0.842
	fbsp2-1-1																																				

Table A4. The values of proposed damage indices for triple-damage scenarios.

		Triple-Damage Scenario																	
		Left_Middle_Right (T_LMR)																	
		Cr 15%						**Cr 30%**						**Cr 50%**					
Wavelet Families		**DI_MW**			**DI_SW**			**DI_MW**			**DI_SW**			**DI_MW**			**DI_SW**		
		L	**M**	**R**	**L**	**M**	**R**	**L**	**M**	**R**	**L**	**M**	**R**	**L**	**M**	**R**	**L**	**M**	**R**
db	db1 = haar				0.957	1.214	1.401				1.387	1.468	1.745				1.549	1.715	1.798
	db2				1.308	1.426	1.605				1.461	1.552	1.756				1.574	1.68	1.74
	db3																		
	db4				0.795	0.997	1.161				1.101	1.176	1.396				1.23	1.354	1.421
	db5				0.943	1.161	1.317				1.343	1.406	1.661				1.485	1.654	1.717
	db6				1.025	1.168	1.302				1.232	1.293	1.48				1.327	1.442	1.49
	db7																		
	db8	0.5973	0.5971	0.7288													0.705	0.779	0.834
	db9				1.023	1.215	1.362				1.366	1.425	1.66				1.484	1.644	1.692
	db10	1.1765	1.1445	1.3107				0.8996	0.9899	1.0631	1.104	1.143	1.371	0.9097	0.926	0.892	1.219	1.382	1.432
sym	**sym2**				1.113	1.214	1.366				1.243	1.32	1.494				1.339	1.43	1.48
	sym3																		
	sym4										0.615	0.671	0.784				0.685	0.731	0.775
	sym5				0.855	0.991	1.106				1.121	1.155	1.361				1.21	1.33	1.4
	sym6																		
	sym7				1.102	1.254	1.339				1.326	1.385	1.559				1.411	1.536	1.579
	sym8	0.6391	0.5977	0.7178															

Table A4. *Cont.*

		Triple-Damage Scenario																	
		Left_Middle_Right (T_LMR)																	
		Cr 15%						**Cr 30%**						**Cr 50%**					
Wavelet Families		**DI_MW**			**DI_SW**			**DI_MW**			**DI_SW**			**DI_MW**			**DI_SW**		
		L	**M**	**R**	**L**	**M**	**R**	**L**	**M**	**R**	**L**	**M**	**R**	**L**	**M**	**R**	**L**	**M**	**R**
coif	coif1	0.6558	0.6459	0.7964													0.614	0.63	0.669
	coif2	0.5773	0.54	0.6616															
	coif3	0.6198	0.5733	0.6908															
	coif4																		
	coif5																		
bior	bior1.1																		
	bior1.3	0.6964	0.667	0.8248															
	bior1.5	0.6982	0.6742	0.8357															
	bior2.2																		
	bior2.4																0.597	0.625	0.654
	bior2.6				0.611	0.697	0.779				0.623	0.698	0.786				0.682	0.715	0.737
	bior2.8				0.691	0.765	0.807				0.704	0.768	0.848				0.75	0.804	0.794
	bior3.1				1.175	1.393	1.542				1.571	1.635	1.895	0.6992	0.7343	0.7973	1.703	1.877	1.934
	bior3.3										0.664	0.686	0.796	0.7193	0.7568	0.821	0.716	0.793	0.817
	bior3.5							0.6127	0.7272	0.8901				0.7357	0.775	0.8398	0.583	0.646	0.665
	bior3.7							0.627	0.7419	0.9067				0.7508	0.7914	0.8566			
	bior3.9							0.6411	0.7563	0.9227				0.7653	0.8071	0.8723			
	bior4.4	0.6223	0.5807	0.7096															
	bior5.5																		
	bior6.8																		

Table A4. *Cont.*

		Triple-Damage Scenario																	
		Left_Middle_Right (T_LMR)																	
		Cr 15%						Cr 30%						Cr 50%					
Wavelet Families		DI_MW			DI_SW			DI_MW			DI_SW			DI_MW			DI_SW		
		L	M	R	L	M	R	L	M	R	L	M	R	L	M	R	L	M	R
rbio	rbio1.1																		
	rbio1.3													0.7039	0.7393	0.8022			
	rbio1.5													0.6195	0.6442	0.7013			
	rbio2.2																		
	rbio2.4																		
	rbio2.6																		
	rbio2.8																		
	rbio3.1													0.8252	0.8763	0.9408			
	rbio3.3																		
	rbio3.5							0.7267	0.8691	1.1027				0.9121	0.9773	1.088			
	rbio3.7													0.6465	0.6686	0.7447			
	rbio3.9																		
	rbio4.4																		
	rbio5.5																		
	rbio6.8																		
meyr	meyr																		
dmey	dmey																		

Table A4. *Cont.*

		Triple-Damage Scenario																	
		Left_Middle_Right (T_LMR)																	
		Cr 15%						Cr 30%						Cr 50%					
Wavelet Families		**DI_MW**			**DI_SW**			**DI_MW**			**DI_SW**			**DI_MW**			**DI_SW**		
		L	**M**	**R**	**L**	**M**	**R**	**L**	**M**	**R**	**L**	**M**	**R**	**L**	**M**	**R**	**L**	**M**	**R**
gaus	gaus1				0.801	0.979	1.102				1.135	1.183	1.389				1.247	1.386	1.435
	gaus2																		
	gaus3																		
	gaus4																		
	gaus5																		
	gaus6																		
	gaus7																		
	gaus8																		
mexh	mexh										0.596	0.637	0.762				0.662	0.742	0.768
morl	morl																		
cgau	cgau1										0.636	0.666	0.78				0.699	0.772	0.803
	cgau2																		
	cgau3																		
	cgau4	0.6918	0.6668	0.8234															
	cgau5																		
shan	shan1-1.5																		
	shan1-1																		
	shan1-0.5	0.9554	1.104	1.2164	0.995	1.209	1.342	1.2676	1.3055	1.518	1.436	1.48	1.737	1.3568	1.5241	1.5432	1.567	1.757	1.809
	shan1-0.1	0.9562	1.1054	1.2201	0.973	1.186	1.32	1.2659	1.3055	1.5193	1.413	1.457	1.712	1.3557	1.5231	1.542	1.544	1.733	1.786
	shan2-3																		

Table A4. *Cont.*

		Triple-Damage Scenario																	
		Left_Middle_Right (T_LMR)																	
		Cr 15%						Cr 30%						Cr 50%					
Wavelet Families		DI_MW			DI_SW			DI_MW			DI_SW			DI_MW			DI_SW		
		L	M	R	L	M	R	L	M	R	L	M	R	L	M	R	L	M	R
fbsp	fbsp1-1-1.5																		
	fbsp1-1-1																		
	fbsp1-1-0.5	0.9554	1.104	1.2164				1.2676	1.3055	1.518	0.689	0.71	0.833	1.3568	1.5241	1.5432	0.752	0.843	0.868
	fbsp2-1-1																		
	fbsp2-1-0.5																		
	fbsp2-1-0.1	0.9497	1.0996	1.2136	0.983	1.196	1.328	1.262	1.3009	1.5144	1.425	1.468	1.725	1.3523	1.5193	1.5392	1.556	1.747	1.799
cmor	cmor1-1.5																		
	cmor1-1																		
	cmor1-0.5							1.0334	1.0792	1.328				1.1762	1.3616	1.4047			
	cmor1-0.1							1.2745	1.3088	1.5724	0.865	0.872	1.016	1.4186	1.6222	1.6728	0.929	1.056	1.072

References

1. Sarmadi, H.; Entezami, A.; De Michele, C. Probabilistic Data Self-Clustering Based on Semi-Parametric Extreme Value Theory for Structural Health Monitoring. *Mech. Syst. Signal Process.* **2023**, *187*, 109976. [CrossRef]
2. Coraça, E.M.; Ferreira, J.V.; Nóbrega, E.G.O. An Unsupervised Structural Health Monitoring Framework Based on Variational Autoencoders and Hidden Markov Models. *Reliab. Eng. Syst. Saf.* **2023**, *231*, 109025. [CrossRef]
3. Farrar, C.R.; Worden, K. *Structural Health Monitoring: A Machine Learning Perspective*; John Wiley & Sons: Hoboken, NJ, USA, 2012; ISBN 9781119994336.
4. Kamariotis, A.; Chatzi, E.; Straub, D. A Framework for Quantifying the Value of Vibration-Based Structural Health Monitoring. *Mech. Syst. Signal Process.* **2023**, *184*, 109708. [CrossRef]
5. Peng, X.; Yang, Q. Damage Detection in Beam-like Structures Using Static Shear Energy Redistribution. *Front. Struct. Civ. Eng.* **2023**, *16*, 1552–1564. [CrossRef]
6. Rytter, A. Vibration Based Inspection of Civil Engineering Structures. Ph.D. Thesis, Department of Building Technology and Structural Engineering, Aalborg University, Aalborg, Denmark, 1993.
7. Comanducci, G.; Magalhães, F.; Ubertini, F.; Cunha, Á. On Vibration-Based Damage Detection by Multivariate Statistical Techniques: Application to a Long-Span Arch Bridge. *Struct. Health Monit.* **2016**, *15*, 505–524. [CrossRef]
8. Lucà, F.; Manzoni, S.; Cigada, A.; Frate, L. A Vibration-Based Approach for Health Monitoring of Tie-Rods under Uncertain Environmental Conditions. *Mech. Syst. Signal Process.* **2022**, *167*, 108547. [CrossRef]
9. Le-Ngoc, V.; Vuong-Cong, L.; Pham-Bao, T.; Ngo-Kieu, N. Damage Detection of the Beam Under Moving Load by Using a Variation of Power Spectrum Density. In *Lecture Notes in Mechanical Engineering*; Springer: Berlin/Heidelberg, Germany, 2023; pp. 207–219, ISBN 9789811948343.
10. Hanumanthappa, S. A New Structural Damage Detection Method for Cantilever Beam Using Generalized Flexibility Quotient Difference Method. *J. Vib. Eng. Technol.* **2022**, *11*, 1525–1533. [CrossRef]
11. Nguyen, T.Q. Damage Detection in Beam Structures Using Bayesian Deep Learning and Balancing Composite Motion Optimization. *Structures* **2022**, *39*, 98–114. [CrossRef]
12. Huang, J.; Deng, T.; Cao, M.; Qian, X.; Bayat, M. A Feature of Mechanics-Driven Statistical Moments of Wavelet Transform-Processed Dynamic Responses for Damage Detection in Beam-Type Structures. *Appl. Sci.* **2022**, *12*, 11561. [CrossRef]
13. Pooya, S.M.H.; Massumi, A. A Novel Damage Detection Method in Beam-like Structures Based on the Relation between Modal Kinetic Energy and Modal Strain Energy and Using Only Damaged Structure Data. *J. Sound Vib.* **2022**, *530*, 116943. [CrossRef]
14. Worden, K.; Farrar, C.R.; Haywood, J.; Todd, M. A Review of Nonlinear Dynamics Applications to Structural Health Monitoring. *Struct. Control. Health Monit.* **2008**, *15*, 540–567. [CrossRef]
15. Zou, Y.; Tong, L.; Steven, G.P. Vibration-Based Model-Dependent Damage (Delamination) Identification and Health Monitoring for Composite Structures—A Review. *J. Sound Vib.* **2000**, *230*, 357–378. [CrossRef]
16. García, D.; Trendafilova, I. A Multivariate Data Analysis Approach towards Vibration Analysis and Vibration-Based Damage Assessment: Application for Delamination Detection in a Composite Beam. *J. Sound Vib.* **2014**, *333*, 7036–7050. [CrossRef]
17. Jahangiri, M.; Hadianfard, M.A. Vibration-Based Structural Health Monitoring Using Symbiotic Organism Search Based on an Improved Objective Function. *J. Civ. Struct. Health Monit.* **2019**, *9*, 741–755. [CrossRef]
18. Larsen, G.C.; Berring, P.; Tcherniak, D.; Nielsen, P.H.; Branner, K. Effect of a Damage to Modal Parameters of a Wind Turbine Blade. In Proceedings of the 7th European Workshop on Structural Health Monitoring, EWSHM 2014—2nd European Conference of the Prognostics and Health Management (PHM) Society, Nantes, Frances, 8–11 July 2014; pp. 261–269.
19. Pardoen, G.C. Effect of Delamination on the Natural Frequencies of Composite Laminates. *J. Compos. Mater.* **1989**, *23*, 1200–1215. [CrossRef]
20. Kessler, S.S.; Spearing, S.M.; Atalla, M.J.; Cesnik, C.E.S.; Soutis, C. Damage Detection in Composite Materials Using Frequency Response Methods. *Compos. Part B Eng.* **2002**, *33*, 87–95. [CrossRef]
21. Carden, E.P.; Fanning, P. Vibration Based Condition Monitoring: A Review. *Struct. Health Monit.* **2004**, *3*, 355–377. [CrossRef]
22. Garcia, D.; Palazzetti, R.; Trendafilova, I.; Fiorini, C.; Zucchelli, A. Vibration-Based Delamination Diagnosis and Modelling for Composite Laminate Plates. *Compos. Struct.* **2015**, *130*, 155–162. [CrossRef]
23. Ooijevaar, T.H.; Loendersloot, R.; Warnet, L.L.; de Boer, A.; Akkerman, R. Vibration Based Structural Health Monitoring of a Composite T-Beam. *Compos. Struct.* **2010**, *92*, 2007–2015. [CrossRef]
24. Loendersloot, R.; Ooijevaar, T.H.; Warnet, L.; de Boer, A.; Akkerman, R. Vibration Based Structural Health Monitoring and the Modal Strain Energy Damage Index Algorithm Applied to a Composite T-Beam. In *Vibration and Structural Acoustics Analysis*; Springer: Dordrecht, The Netherlands, 2011; pp. 121–150.
25. Jyrki, K.; Kari, S.; Anthony, E. Vibration-Based Structural Health Monitoring of a Simulated Beam with a Breathing Crack. *Key Eng. Mater.* **2013**, *569–570*, 1093–1100. [CrossRef]
26. Ho, D.-D.; Thanh-Cao, L. Structural Health Monitoring of Prestressed Concrete Beams by Vibration- and Impedance-Based Smart Technologies. In Proceedings of the IOP Conference Series: Materials Science and Engineering, Chennai, India, 16–17 September 2020; Volume 849, p. 012086.
27. Huang, Y.; Meyer, D.; Nemat-Nasser, S. Damage Detection with Spatially Distributed 2D Continuous Wavelet Transform. *Mech. Mater.* **2009**, *41*, 1096–1107. [CrossRef]

28. Newland, D.E. *An Introduction to Random Vibrations, Spectral & Wavelet Analysis*; Courier Corporation: New York, NY, USA, 1993; ISBN 0486136965.
29. Wang, W.J.; McFadden, P.D. Application of Orthogonal Wavelets to Early Gear Damage Detection. *Mech. Syst. Signal Process.* **1995**, *9*, 497–507. [CrossRef]
30. Surace, C.; Ruotolo, R. Crack Detection of a Beam Using the Wavelet Transform. In Proceedings of the 12th International Modal Analysis Conference; Spie International Society for Optical, Honolulu, HI, USA, 32 January–3 February 1994; Volume 1141, pp. 1141–1167.
31. Salehian, A. Identifying the Location of a Sudden Damage in Composite Laminates Using Wavelet Approach. In Proceedings of the Submitted to 16th ASCE Conference, Baltimore, Maryland, 13–16 July 2003; University of Washington: Seattle, WA, USA, 2003; p. 79.
32. Yan, Y.J.; Yam, L.H. Detection of Delamination Damage in Composite Plates Using Energy Spectrum of Structural Dynamic Responses Decomposed by Wavelet Analysis. *Comput. Struct.* **2004**, *82*, 347–358. [CrossRef]
33. Shi, A.; Yu, X.H. Structural Damage Detection Using Artificial Neural Networks and Wavelet Transform. In Proceedings of the CIMSA 2012—2012 IEEE International Conference on Computational Intelligence for Measurement Systems and Applications, Tianjin, China, 2–4 July 2012; pp. 7–11.
34. Fallahian, M.; Ahmadi, E.; Khoshnoudian, F. A Structural Damage Detection Algorithm Based on Discrete Wavelet Transform and Ensemble Pattern Recognition Models. *J. Civ. Struct. Health Monit.* **2022**, *12*, 323–338. [CrossRef]
35. Kaur, K.; Alamdari, M.M.; Chang, K.C.; Kim, C.W.; Atroshchenko, E. Damage Detection and Localization for Indirect Bridge Monitoring Exploiting Adversarial Autoencoder and Wavelet Transform. In *Lecture Notes in Civil Engineering*; Springer International Publishing: Cham, Switzerland, 2023; Volume 253, pp. 657–667, ISBN 9783031072536.
36. Pradeep, P.A.; Thankachan, P.; Pillai, T.M.M. Vibration-Based Damage Detection on Plate Structure Using Wavelet Transform Method. In *Structural Integrity*; Springer International Publishing: Cham, Switzerland, 2023; Volume 26, pp. 477–487.
37. Ruan, Z.G.; Ying, Z.G. Comparative Study of Structural Anomaly Diagnosis Based on ANN Model Using Random Displacement and Acceleration Responses with Incomplete Measurements. *Sensors* **2022**, *22*, 4128. [CrossRef]
38. Mallat, S. *A Wavelet Tour of Signal Processing*; Academic Press: London, UK, 1999.
39. Ovanesova, A.V.; Suárez, L.E. Applications of Wavelet Transforms to Damage Detection in Frame Structures. *Eng. Struct.* **2004**, *26*, 39–49. [CrossRef]
40. Jahangir, H.; Esfahani, M.R. Structural Damage Identification Based on Modal Data and Wavelet Analysis. In Proceedings of the 3rd National Conference on Earthquake & Structure, Kerman, Iran, 17–18 October 2012.
41. Gao, R.X.; Yan, R. *Wavelets: Theory and Applications for Manufacturing*; Springer: Boston, MA, USA, 2011; ISBN 978-1-4419-1544-3.
42. Baghiee, N.; Reza Esfahani, M.; Moslem, K. Studies on Damage and FRP Strengthening of Reinforced Concrete Beams by Vibration Monitoring. *Eng. Struct.* **2009**, *31*, 875–893. [CrossRef]
43. Jahangir, H.; Hasani, H.; Esfahani, M.R. Wavelet-Based Damage Localization and Severity Estimation of Experimental RC Beams Subjected to Gradual Static Bending Tests. *Structures* **2021**, *34*, 3055–3069. [CrossRef]
44. Smith, M. *ABAQUS/Standard User's Manual, Version 6.9*; Simulia: Providence, RI, USA, 2009.
45. Pappalardo, C.M.; Guida, D. System identification and experimental modal analysis of a frame structure. *Eng. Lett.* **2018**, *26*, 1–13.
46. Sohn, H.; Czarnecki, J.A.; Farrar, C.R. Structural Health Monitoring Using Statistical Process Control. *J. Struct. Eng.* **2000**, *126*, 1356–1363. [CrossRef]
47. Sadeghi, F.; Mousavi, M.; Zhu, X.; Rashidi, M.; Samali, B.; Gandomi, A.H. Damage Detection of Composite Beams via Variational Mode Decomposition of Shear-Slip Data. *J. Struct. Eng.* **2023**, *149*, 04022226. [CrossRef]
48. Khan, S.M.; Hanif, M.U.; Khan, A.; Hassan, M.U.; Javanmardi, A.; Ahmad, A. Damage Assessment of Reinforced Concrete Beams Using Cost-Effective MEMS Accelerometers. *Structures* **2022**, *41*, 602–618. [CrossRef]
49. Sun, Z.; Chang, C.C. Statistical Wavelet-Based Method for Structural Health Monitoring. *J. Struct. Eng.* **2004**, *130*, 1055–1062. [CrossRef]
50. Hanif, M.U.; Ibrahim, Z.; Ghaedi, K.; Hashim, H.; Javanmardi, A. Damage Assessment of Reinforced Concrete Structures Using a Model-Based Nonlinear Approach—A Comprehensive Review. *Constr. Build. Mater.* **2018**, *192*, 846–865. [CrossRef]
51. Han, J.-G.; Ren, W.-X.; Sun, Z.-S. Wavelet Packet Based Damage Identification of Beam Structures. *Int. J. Solids Struct.* **2005**, *42*, 6610–6627. [CrossRef]
52. Daubechies, I. *Ten Lectures on Wavelets*; SIAM: Philadelphia, PA, USA, 1992.
53. Abry, P. *Ondelettes et Turbulence. Multirésolutions, Algorithmes de Décomposition, Invariance D'échelles*; Nouveaux essais; Diderot multimédia: Paris, France, 1997; ISBN 2-84134-064-3.
54. Teolis, A. *Computational Signal Processing with Wavelets*; Birkhäuser Boston: Boston, MA, USA, 1998.